Journal of Asian Earth Sciences xxx (2014) xxx–xxx

Contents lists available at ScienceDirect

Journal of Asian Earth Sciences

journal homepage: www.elsevier.com/locate/jseaes

Apatite fission-track thermochronological constraints on the pattern of late Mesozoic–Cenozoic uplift and exhumation of the Qinling Orogen, central China

Hong Chen [a,b], Jianmin Hu [a,b,*], Guoli Wu [c], Wei Shi [a,b], Yingying Geng [d], Hongjie Qu [a,b]

[a] Institute of Geomechanics, Chinese Academy of Geological Sciences, Beijing 100081, China
[b] Key Laboratory of Paleomagnetism and Tectonic Reconstruction of Ministry of Land and Resources, Beijing 100081, China
[c] Institute of Geology and Geophysics, Chinese Academy of Sciences, Beijing 100029, China
[d] CNNC Beijing Research Institute of Uranium Geology, Beijing 100029, China

ARTICLE INFO

Article history:
Received 30 June 2014
Received in revised form 28 September 2014
Accepted 3 October 2014
Available online xxxx

Keywords:
Qinling Orogen
Apatite fission-track analysis
Propagation of uplift and exhumation
Intracontinental deformation

ABSTRACT

The Qinling Orogen of central China was formed by intracontinental collision between the North and South China Blocks. The orogen comprises several micro-blocks bounded by sutures and faults, and has undergone long-term intracontinental deformation since the Late Triassic. The micro-blocks include the southern margin of the North China Block (S-NCB), the Northern Qinling Belt (NQB), the Southern Qinling Belt (SQB), and the northern margin of the South China Block (N-SCB). Under a uniform tectonic setting in late Mesozoic–Cenozoic, these micro-blocks have been subjected to a range of deformation styles, as demonstrated by their structural deformation, history of magmatism, and the development of sedimentary basins. To investigate the differences among the micro-blocks and to quantify their uplift and exhumation, we obtained 45 rock samples from eight Mesozoic granites in these micro-blocks, and conducted apatite fission-track (AFT) thermochronological modeling. The results reveal that the Qinling Orogen underwent four distinct stages of rapid cooling histories during the late Mesozoic–Cenozoic, and showed variation in uplift and exhumation whereby the intracontinental deformation started in the south (the N-SCB) and propagated to the north (S-NCB). In the first stage, during the Late Jurassic–Early Cretaceous (ca. 160–120 Ma), rock cooling occurred mainly in the N-SCB, attributed to the clockwise rotation and northward subduction of the South China Block beneath the Qinling Orogen. In the second stage, compression- and extension-related uplift was initiated during the late Early Cretaceous–early Late Cretaceous (ca. 120–90 Ma) in the SQB, consistent with the southward subduction of the North China Block and broadly extensional deformation in the eastern China continent. In the third stage, a gentle regional-scale cooling event that occurred during the latest Cretaceous–Paleocene (ca. 90–50 Ma) started in the NQB and became widespread in the Qinling Orogen. This regional-scale uplift and exhumation event was probably a response to the opposite polarity subduction beneath the Qinling Orogen combined with the effects of subduction of the Pacific Plate from the southeast. The fourth stage (Eocene–Oligocene, ca. 50–20 Ma) was marked by another phase of rapid cooling in the S-NCB, the NQB, and the NW-SQB, and is interpreted as being cause by the eastward tectonic escape of Tibetan Plateau related to India–Asia collision. Furthermore, the record of variable timings and rates of cooling of these micro-blocks, together with regional structural analysis, indicates that the late Mesozoic–Cenozoic intracontinental deformation in the Qinling Orogen was characterized by a spatiotemporally variable and propagating-style uplift and exhumation of the micro-blocks, and the predominant deformation was through displacement across various boundary sutures and faults.

© 2014 Elsevier Ltd. All rights reserved.

1. Introduction

The Qinling Orogen is a Mesozoic intercollisional orogen that formed as a result of approximately south–north-oriented convergence and collision in the Proto-Tethys during the Neoproterozoic and in the Paleo-Tethys during the late Paleozoic (Dong et al., 2011a; Meng and Zhang, 2000; Yin and Nie, 1993, 1996; Zhang

* Corresponding author at: Institute of Geomechanics, Chinese Academy of Geological Sciences, Beijing 100081, China. Tel.: +86 (0)10 88815003.
E-mail address: jianminhu@vip.sina.com (J. Hu).

http://dx.doi.org/10.1016/j.jseaes.2014.10.004
1367-9120/© 2014 Elsevier Ltd. All rights reserved.

Please cite this article in press as: Chen, H., et al. Apatite fission-track thermochronological constraints on the pattern of late Mesozoic–Cenozoic uplift and exhumation of the Qinling Orogen, central China. Journal of Asian Earth Sciences (2014), http://dx.doi.org/10.1016/j.jseaes.2014.10.004

et al., 1996, 2001). This was followed by intercontinental collision and intracontinental deformation after closure of the Mianlue paleo-oceanic basin during the early Mesozoic (Dong et al., 2011a; Yin and Nie, 1993; Zhang et al., 2004). This prolonged tectonic history led to the final formation of the Qinling Orogen as a collage of micro-blocks, which are named the southern margin of the North China Block (S-NCB), the Northern Qinling Belt (NQB), the Southern Qinling Belt (SQB), and the northern margin of the South China Block (N-SCB). These micro-blocks constitute a south–north tectonic zoning of the Qinling Orogen (Fig. 1; Dong et al., 2011a; Zhang et al., 1996, 2001, 2004). Since the early Mesozoic, the Qinling Orogen evolved into a huge intracontinental deformation belt with an east–west length of ca. 1000 km and extending from the western Qinling to the Dabie Orogen, as revealed by studies of the structure, Mesozoic basins, and geochronology and geochemistry of the micro-blocks of the Qinling Orogen (Fig. 2; Chen et al., 2010; Dong et al., 2011a; Hu et al., 2012; Meng et al., 2007; Meng and Zhang, 2000; Li et al., 2007; Ratschbacher et al., 2003; Shi et al., 2012, 2013; Wang et al., 2011a; Yin and Nie, 1993, 1996; Zhang et al., 2001, 2010). For the intracontinental deformation, various fission-track and U–Th/He thermochronological investigations of the apatite and zircon have indicated that the Qinling Orogen experienced an intricate pattern of postorogenic uplift and exhumation during the Mesozoic–Cenozoic (Enkelmann et al., 2006; Hu et al., 2006a, 2012; Li et al., 2010a; Liu et al., 2009, 2013; Shen et al., 2007; Tian et al., 2010; Wan et al., 2000, 2005; Wang et al., 2011b; Xu et al., 2005, 2010; Yang et al., 2013; Yin et al., 2001). The southern Qinling orogen has been uplifted since the Triassic–Jurassic (Hu et al., 2012; Shen et al., 2007; Xu et al., 2010; Yang et al., 2013), but the northern Qinling Orogen uplifted only since the Cenozoic (Enkelmann et al., 2006; Hu et al., 2006a; Liu et al., 2013), and the rapid cooling documented in the southwestern Qinling Orogen started during the late Miocene (Enkelmann et al., 2006). The variable timings of uplift and exhumation at different locations in the Qinling Orogen represent differences in the pattern and timing of tectonism not only from south to north (Hu et al., 2006a; Liu et al., 2013) but also from east to west (Enkelmann et al., 2006).

However, the early studies usually established the timing and rate of cooling/exhumation for single granitic pluton (Hu et al., 2012; Li et al., 2010a; Liu et al., 2009; Shen et al., 2007; Tian et al., 2010; Wan et al., 2000, 2005; Xu et al., 2005, 2010; Yin et al., 2001) or basins (Wang et al., 2011b), and was deficient in the thermal modeling data. Recently, there are some studies on the regional evolution of Qinling Orogen based on the north–south transects (Hu et al., 2006a), east–west different (Liu et al., 2013), individual micro-block of S-NCB and NQB (Liu et al., 2013) or N-SCB (Yang et al., 2013), and have also discussed the tectonic context of different uplift and exhumation stages (Enkelmann et al., 2006; Hu et al., 2006a; Liu et al., 2013; Yang et al., 2013).

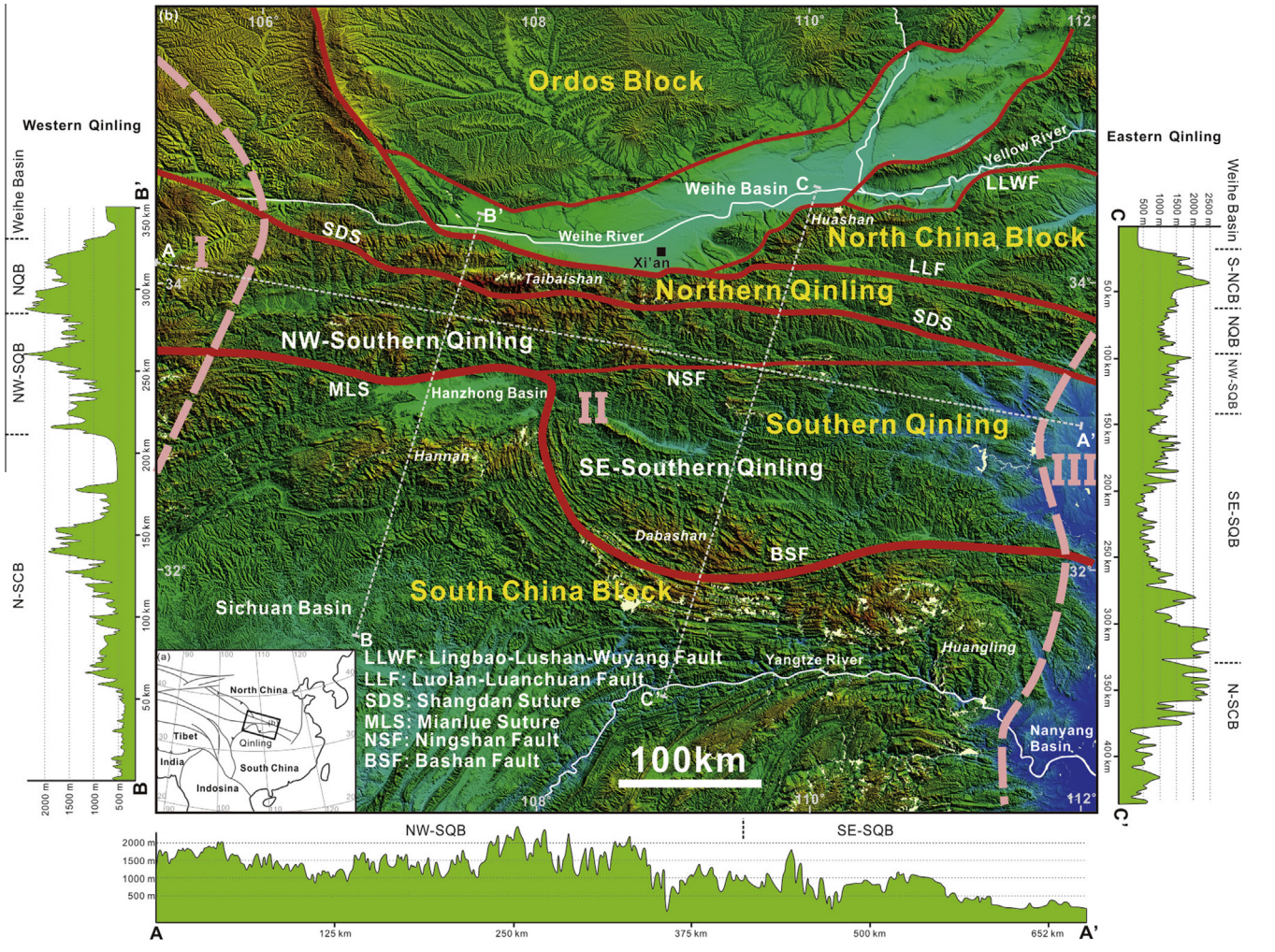

Fig. 1. Topography, topographic profiles, and tectonic units of the Qinling Orogen. The numbers I, II, and III indicate the three topographic steps, and the pink lines represent the boundaries between the steps.

Please cite this article in press as: Chen, H., et al. Apatite fission-track thermochronological constraints on the pattern of late Mesozoic–Cenozoic uplift and exhumation of the Qinling Orogen, central China. Journal of Asian Earth Sciences (2014), http://dx.doi.org/10.1016/j.jseaes.2014.10.004

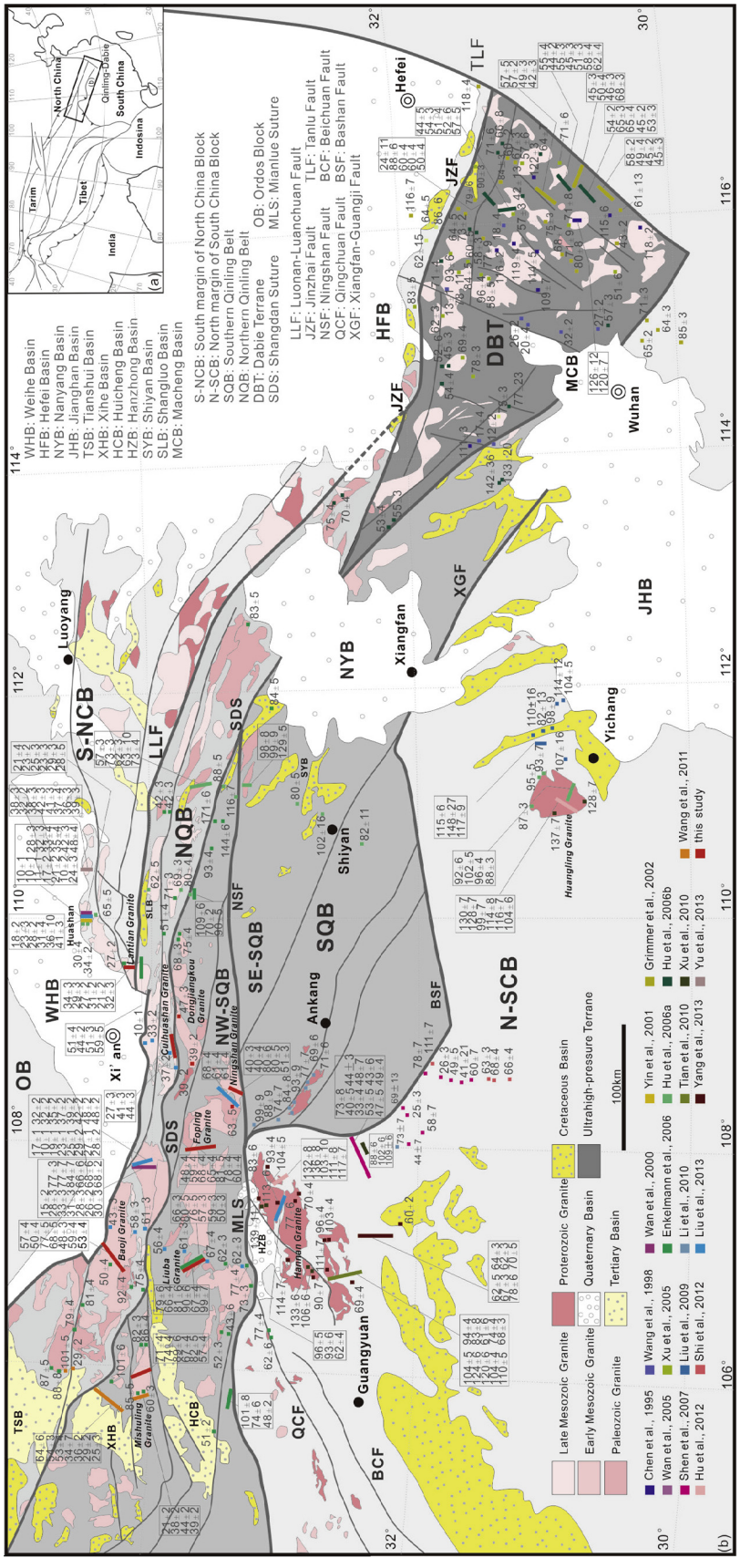

Fig. 2. Regional tectonic framework and apatite fission-track ages in the Qinling Orogen and Dabie Terrane.

Previous studies were dominantly on the individual pluton, and the spatial coverage is limited to reveal the uplift and exhumation for the entire Qinling Orogen (Fig. 2). Although the existing data at different location have showed that the micro-blocks of the Qinling Orogen experienced different uplift and exhumation process, the summary for the evolution of the Qinling Orogen was insufficiency at present. Especially for the Meso-Cenozoic tectonic deformation and faulting activity (Hu et al., 2012; Ratschbacher et al., 2003; Yin, 2010; Yin and Nie, 1993; Zhang et al., 2001), the previous data were lack of comparative, which resulted the preceding conclusions were still considerable debate about the pattern of uplift and deformation in the Qinling Orogen. Three stages (e.g. Late Triassic–Early Jurassic, Late Cretaceous–Eocene, and Eocene–Miocene) of uplift and exhumation with a northward-younging pattern has been identified from the Late Triassic to the Cenozoic (Hu et al., 2006a), not including the Hannan–Micangshan massif and Huangling Granite uplifted in the Late Jurassic–Early Cretaceous (Hu et al., 2012; Tian et al., 2010; Yang et al., 2013). Regional-scale uplift and exhumation did not occur in the S-NCB during the Cretaceous, but initiated during the early Cenozoic (Liu et al., 2013; Wan et al., 2005), and also for the uplift and exhumation of the Hannan–Micangshan massif (Yang et al., 2013). The timing of uplift and exhumation of the N-SCB differs from the southern Dabashan belt to the eastern and western of the N-SCB (Shen et al., 2007; Shi et al., 2012; Xu et al., 2010). Rapid late-Cenozoic cooling/exhumation initiated not only in the southwestern Qinling Orogen (Enkelmann et al., 2006) but also in the S-NCB (Liu et al., 2013).

It is clear that the timing and spatial patterns of uplift and exhumation in the Qinling Orogen are still not completely resolved, because of the lack of geochronological data, especially low-temperature thermochronological data, such as the western of the NQB and center of the SQB (Fig. 2), or thermal modeling data, such as the western of SQB. Furthermore, the causes of the differences in the timing and amount/rate of uplift and exhumation of the various constituent micro-blocks have not been well quantified. The previous studies have indicated that the evolution of the micro-blocks was different. Here, we dominantly focus on the uplift and exhumation history of the entire Qinling Orogen and on the differences between the various micro-blocks. The existing apatite fission-track (AFT) data was dominant in the previous thermchronological research, and the data was difficult to contrast related to the tectonic location, lithology and age of the samples, the analysis method and lab, so we need the AFT thermochronological modeling for valuable comparison with the previous data. By combining the AFT age and thermal modeling with geological information on regional structure, sedimentary basins, magmatism, and geophysical characteristics, we proposed four-stage uplift and exhumation history of the Qinling Orogen that incorporates differences between the various micro-blocks of the orogen, and that confirms the causes of these differences.

2. Tectonic framework

The Qinling Orogen extends about 1000 km from west to east, and crosses the three-step macrotopographic configuration of central China (Figs. 1 and 2; Zhang et al., 2001). The orogen locates mainly in the first and second topographic steps, whereas the Dabie Terrane is located in the third topographic step, which is separated from the Qinling Orogen by the Nanyang Basin (Fig. 1). The Qinling Orogen separates north- and south-directed drainage systems (Zhang et al., 2001).

The Qinling Orogen is located between the North and South China blocks, and is bounded by the Lingbao–Lushan–Wuyang Fault (LLWF) to the north and the Mianlue–Bashan–Xiangguang Fault (MBXF) to the south (Dong et al., 2011a). The orogen experienced several stages of Tethyan tectonism range from the Neoproterozoic to the Early–Middle Triassic, and intracontinental orogenesis since the Late Triassic (Dong et al., 2011a; Meng and Zhang, 1999; Yin and Nie, 1993, 1996; Zhang et al., 1996). There are two important sutures in the orogen: the Shangdan Suture in the north and the Mianlue Suture in the south (Fig. 2; Dong et al., 2011a; Meng and Zhang, 2000; Yin and Nie, 1993, 1996; Zhang et al., 1989, 1996, 2004). The Shangdan Suture formed as a result of the closure of the Proto-Tethys between the North China and South China blocks during the early Paleozoic (Dong et al., 2011b; Zhang et al., 1989, 2004). The Mianlue Suture formed from the closure of the Paleo-Tethys oceanic basin in the Qinling Orogen during Early–Middle Triassic (Dong et al., 1999; Lai et al., 2004; Zhang et al., 1996). The Luonan–Luanchuan Fault (LLF) forms the southern boundary of the North China Block, the Bashan Fault separates the Dabashan thrust-belt from the northern margin of the South China Block, and the Xiangfan–Guangji Fault (XGF) separates the northern margin of the South China Block from the Dabie Terrane (Dong et al., 2011a). The Qinling Orogen can be divided into four micro-blocks: the southern margin of the North China Block (S-NCB), the Northern Qinling Belt (NQB), the Southern Qinling Belt (SQB) and the northern margin of the South China Block (N-SCB) (Dong et al., 2011a; Zhang et al., 2001). The Ningshan Fault separates the SQB into the NW-SQB and SE-SQB, which differ from each other in terms of basement rocks and magmatism (Hu et al., 2011).

The S-NCB is located to the north of the LLF and to the south of both the Weihe Basin and the LLWF (Figs. 1 and 2), and is characterized by Neoarchean to Neoproterozoic basement rocks (Meng and Zhang, 2000) that are overlain by a Mesoproterozoic rift-related rock system and succeeding Cambrian to Ordovician passive continental margin sequences (Dong et al., 2011a). Numerous Cretaceous granitoid plutons (e.g., the Lantian, Huashan and Wenyu granitoids) was intruded in the S-NCB during the intracontinental deformation stage (Dong et al., 2011a; Mao et al., 2005; Ye et al., 2006; Zhao et al., 2012). Tertiary basins formed along a NE–SW-trending axis (Ratschbacher et al., 2003).

The NQB is bounded to the south by the Shangdan Suture and to the north by the Weihe Basin and LLF (Fig. 2), and contains mostly Precambrian basement units, Neoproterozoic and early Paleozoic ophiolites, and volcanic-sedimentary assemblages, all of which are unconformably overlain by upper Paleozoic clastic sediments (Dong et al., 2011a; Zhang et al., 2001), and also superimposed by early Mesozoic granite from the syncollisional period and late Mesozoic granite from the intracontinental deformation period (Dong et al., 2011a; Wang et al., 2013). Some WNW–ESE-trending Tertiary basins (e.g., the Shangluo Basin) are developed along the LLF fault in the eastern part of the NQB (Ratschbacher et al., 2003).

The SQB, which is bounded by the Shangdan Suture to the north and the Mianlue–Bashan–Xiangguang Fault (MBXF) to the south, is characterized by two layers: Precambrian basement and overlying layers of Paleozoic–Cenozoic strata (Dong et al., 2011a; Zhang et al., 1996). The composition of the Precambrian basement and the metamorphism of the SE-SQB differ from that of the NW-SQB (Hu et al., 2011). The SE-SQB is characterized by the Proterozoic granite in the Fenghuang dome (Li et al., 2010a,b) and intruded by early Paleozoic mafic dykes in the Dabashan area (Hu et al., 2011; Zhang et al., 2007), whereas the NW-SQB is dominant with early Mesozoic granite (Dong et al., 2011a; Zhang et al., 2008). NE–SW-trending Cretaceous–Tertiary basins (e.g., the Huicheng and Xihe basins) developed in the NW-SQB, whereas NW–SE-trending Cretaceous basins (e.g., the Shiyan basin) developed in the SE-SQB (Ratschbacher et al., 2003).

The northern margin of the South China Block is located to the south of the MBXF, and the outcrops in this margin comprise Proterozoic–Mesozoic strata (Dong et al., 2011a; Shi et al., 2012). Proterozoic granites (e.g., the Hannan and Huangling granites) are

Please cite this article in press as: Chen, H., et al. Apatite fission-track thermochronological constraints on the pattern of late Mesozoic–Cenozoic uplift and exhumation of the Qinling Orogen, central China. Journal of Asian Earth Sciences (2014), http://dx.doi.org/10.1016/j.jseaes.2014.10.004

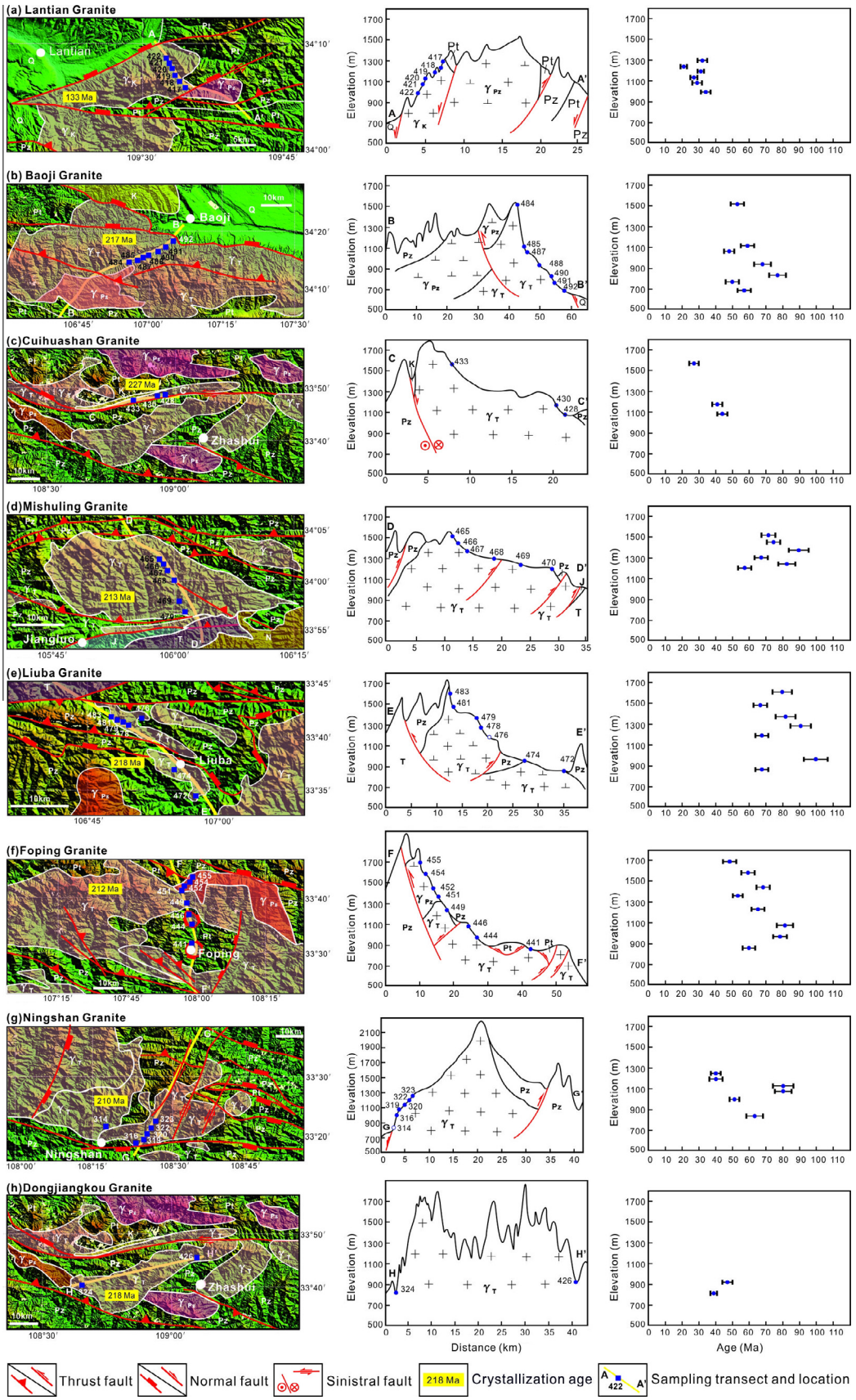

Fig. 3. Geological and topographic background (left), sample profiles (center), and age-elevation schemas (right) for AFT samples of the studied granites (geological map were modified from the 1:250,000 geological maps of Tianshui, Baoji, Xi'an, Tongguan, Nueyang, Hanzhong and Zhen'an). Ages in the age-elevation schemas are plotted with an error of 1σ. Pt: Proterozoic strata, Pz: Paleozoic strata, T: Triassic strata, J: Jurassic strata, K: Cretaceous strata, N: Neogene strata, Q: Quaternary strata, γ_{Pz}: Paleozoic granodiorite, γ_T: Triassic granite, γ_K: Cretaceous granite.

Please cite this article in press as: Chen, H., et al. Apatite fission-track thermochronological constraints on the pattern of late Mesozoic–Cenozoic uplift and exhumation of the Qinling Orogen, central China. Journal of Asian Earth Sciences (2014), http://dx.doi.org/10.1016/j.jseaes.2014.10.004

Table 1
Lithological, chronological, and tectonic setting characteristics of the granitic plutons studied using apatite fission-track dating.

Tectonic belt	Granitic pluton	Lithology	No. of samples	Intrusion setting	Intrusion age (Ma)	References
Southern margin of the North China Block	Lantian	Granite	6	Intra-continent	133(U–Pb)	Wang et al. (2013)
Northern Qinling Belt	Baoji	Granite	7	Post-collision	217(U–Pb)	Lu et al. (1999)
	Cuihuashan	Granite	3	Post-collision	227(U–Pb)	Jiang et al. (2010)
Southern Qinling Belt	Mishuling	Granite	6	Post-collision	213(U–Pb)	Qin et al. (2009)
	Liuba	Granodiorite	7	Post-collision	218(U–Pb)	Zhang et al. (2006)
	Foping	Granite	8	Post-collision	212(U–Pb)	Qin et al. (2008)
					217(U–Pb)	Dong et al. (2012)
	Ningshan	Granite	6	Post-collision	210(U–Pb)	Jiang et al. (2010)
	Dongjiangkou	Granite	2	Post-collision	218(U–Pb)	Jiang et al. (2010)
					219(U–Pb)	Yang et al. (2009)

distributed to both the west and east of the Dabashan (Dong et al., 2011a). NNW–SSE-trending Cretaceous basins (e.g., the Yuanan Basin) are developed to the north of the Jianghan Basin (Shi et al., 2013).

Located to the east of the Qinling Orogen, the Dabie Terrane (DBT) is separated from the orogen by the Nanyang Basin, and is bounded by the Shangdan Suture to the southwest, the Xiangfan–Guangji Fault to the south, and the Jinzhai Fault to the north (Fig. 2). The DBT is characterized by the ultrahigh-pressure Triassic metamorphic rocks and late Mesozoic intrusions (Hacker et al., 2000; Ratschbacher et al., 2000).

3. Apatite fission-track (AFT) thermochronological analysis

3.1. AFT samples

With consideration being given to the sample locations of previous studies, we collected samples for AFT analysis from Mesozoic granites distributed in the different micro-blocks of the Qinling Orogen (Figs. 2 and 3). Forty-five granite samples were collected from eight granitoid plutons in three micro-blocks (Table 1). The Lantian Granite is located in the S-NCB; the Baoji Granite is located in the western of NQB and the Cuihuashan Granite in the eastern of NQB; and the Mishuling, Liuba, Foping, Ningshan, and Dongjiangkou Granites are located from west to east in the SQB (Figs. 2 and 3). Of these eight plutons, the Mishuling and Liuba Granites were chosen to compare with the results of previous studies, especially for completing the thermal modeling (Enkelmann et al., 2006; Wang et al., 2011a); the Ningshan, Cuihuashan, and Lantian Granites were selected to complement previous research and spatial coverage (Enkelmann et al., 2006; Liu et al., 2013); and the Baoji, Foping, and Dongjiangkou granitic plutons were chosen to augment the samples collected in different belts and completed the spatial coverage. For each granitic pluton, the samples were collected from top to bottom of the exposed pluton, with an elevation difference of >50 m between each sample (Table 2; Fig. 3). As all these granitic plutons were intruded during the Early Mesozoic postcollisional and Late Mesozoic intracontinental deformation stages in the Qinling Orogen (Table 1; Dong et al., 2012; Jiang et al., 2010; Lu et al., 1999; Qin et al., 2008, 2009; Wang et al., 2013; Yang et al., 2009; Zhang et al., 2006), they have been overprinted by faults, but most of the samples were collected from the area between pairs of faults, apart from the samples taken from the Liuba and Foping granites (Fig. 3). Therefore, the AFT ages should accurately record the late Mesozoic–Cenozoic uplift and exhumation histories of the orogen.

3.2. AFT testing and thermal modeling

Apatites were separated using conventional methods of crushing rocks and by standard magnetic and heavy-liquid techniques. The experiments were performed at the China University of Geosciences (Beijing, China), and the procedures followed those of Yuan et al. (2007). Individual apatite grains were mounted in epoxy resin on glass slides, and then ground and polished to an optical finish to expose internal grain surfaces. Spontaneous tracks were revealed in 7% HNO_3 for 30 s at 25 °C. All samples were neutron flux irradiated in a well-thermalized 421 reactor of China Institute of Atomic Energy (CIAE) at Beijing. Low-uranium muscovite in intimate contact with these grains was used as an external detector during irradiation. Induced tracks were etched in 40% HF for 20 min at 25 °C. Neutron fluence was determined using a CN5 uranium dosimeter glass. Fission-track densities in both natural and induced fission-track populations were measured in air at 1000× magnification. Only those crystals with prismatic sections that were parallel to the crystallographic *c*-axis were used for analysis (Gleadow et al., 1986, 2002; Green, 1986).

To test whether the ages were from a single population of grains (Galbraith, 1981; Galbraith and Laslett, 1993), errors were calculated using the $P(\chi^2)$ value (Green, 1981). If $P(\chi^2) > 5\%$, the single grain ages are contained in the same age group and the pooled age is used as the age estimate of the sample; whereas if $P(\chi^2) \leqslant 5\%$, the central age (the weighted mean age) will be used (Galbraith, 1981). The weighted mean zeta value for apatite used by the fission-track operator in this study was 389.4 ± 19.2, based on the calibration of sample standards.

The lengths of horizontal confined fission tracks were measured under conditions similar to those used for age determinations. As many track lengths as possible were measured (up to ~100) for each sample. The fission-track ages were calculated using the IUGS-recommended zeta calibration approach and the standard fission-track age equation (Galbraith and Laslett, 1993; Hurford and Green, 1982).

Depending on the fission-track parameters (i.e., ages and lengths) and the geological background of the Mesozoic–Cenozoic evolution (Dong et al., 2011a; Ratschbacher et al., 2003; Yin and Nie, 1993, 1996; Zhang et al., 2001) and cooling history of different areas (Enkelmann et al., 2006; Hu et al., 2006a; Liu et al., 2013; Yang et al., 2013), we restricted the initial conditions for inversion modeling as follows. All of the samples were modeled with three time–temperature (*T*–*t*) constraints, which in order of decreasing temperature were: (1) high temperature (>110 °C greater than total annealing) and old age (older than the oldest single grain age), so that all tracks initially formed could be completely annealed; (2) the AFT partial annealing zone (PAZ) temperature range of 60–110 °C and the AFT pooled age; and (3) lower temperatures of 20–60 °C and youngest pooled age (~20 Ma).

T–*t* paths for each sample were derived through inverse Monte Carlo modeling using HeFTy software (version 1.6.7; Ketcham, 2005, 2009) and by applying the annealing model of Ketcham et al. (1999). We used an initial mean track length of 16.3 μm (Donelick et al., 1999), based on personal calibrations on induced confined track lengths in the Durango apatite standard, and the length reduction in the standard of 0.893. For the *c*-axis projection,

Please cite this article in press as: Chen, H., et al. Apatite fission-track thermochronological constraints on the pattern of late Mesozoic–Cenozoic uplift and exhumation of the Qinling Orogen, central China. Journal of Asian Earth Sciences (2014), http://dx.doi.org/10.1016/j.jseaes.2014.10.004

Please cite this article in press as: Chen, H., et al. Apatite fission-track thermochronological constraints on the pattern of late Mesozoic–Cenozoic uplift and exhumation of the Qinling Orogen, central China. Journal of Asian Earth Sciences (2014), http://dx.doi.org/10.1016/j.jseaes.2014.10.004

ARTICLE IN PRESS

Table 2
Apatite fission-track results for the Qinling Orogen.

Rock mass	Sample	Location	Elevation (m)	No. of grains	ρs (10^5/cm^2)	Ns	ρi (10^5/cm^2)	Ni	ρd (10^5/cm^2)	Nd	$P(x^2)$ (%)	Central age (Ma) (±1σ)	Pooled age (Ma) (±1σ)	Mean length (μm) (±1σ)	No. of lengths
Lantian Granite	DBS417/1	N 34°06′16.5″ E 109°34′09.2″	1301	28	1.025	206	5.049	1024	8.053	5142	94.3	32 ± 3	32 ± 3	12.9 ± 2.2	103
	DBS418/1	N 34°06′57.6″ E 109°33′35.6″	1242	28	1.34	324	10.127	2449	7.969	5142	65	21 ± 2	21 ± 2	13.4 ± 2.0	99
	DBS419/1	N 34°07′27.0″ E 109°33′07.1″	1196	28	2.731	1361	13.462	6709	7.885	5142	91.1	31 ± 2	31 ± 2	13.4 ± 1.6	103
	DBS420/1	N 34°08′12.8″ E 109°32′44.4″	1133	28	0.692	247	3.87	1381	7.801	5142	99.4	27 ± 2	27 ± 2	13.6 ± 1.9	86
	DBS421/1	N 34°08′32.3″ E 109°32′31.0″	1080	28	1.213	208	6.378	1094	7.717	5142	99.5	29 ± 3	29 ± 3	13.7 ± 1.5	64
	DBS422/1	N 34°08′59.0″ E 109°32′10.5″	990	28	0.95	325	4.63	1584	8.472	5142	96.8	34 ± 3	34 ± 3	13.0 ± 1.9	108
Baoji Granite	DBS484/1	N 34°14′50.0″ E 106°56′07.8″	1521	28	2.328	654	7.599	2135	8.892	5142	95.2	53 ± 4	53 ± 4	13.1 ± 1.9	101
	DBS485/1	N 34°15′28.4″ E 106°57′42.8″	1114	28	2.221	695	6.457	2021	8.808	5142	99.2	59 ± 4	59 ± 4	13.0 ± 1.7	112
	DBS487/1	N 34°15′43.1″ E 106°58′14.0″	1066	28	1.465	862	5.151	3031	8.724	5142	80.9	48 ± 3	48 ± 3	13.1 ± 1.9	103
	DBS488/1	N 34°16′07.6″ E 106°59′28.8″	939	28	3.471	769	8.566	1898	8.64	5142	69.4	68 ± 5	68 ± 5	13.0 ± 2.0	93
	DBS490/1	N 34°16′25.9″ E 107°01′12.8″	832	14	13.594	1216	29.401	2630	8.556	5142	16.7	77 ± 5	77 ± 5	12.2 ± 1.8	86
	DBS491/1	N 34°16′37.0″ E 107°02′22.9″	767	28	2.45	439	8.119	1455	8.472	5142	99.1	50 ± 4	50 ± 4	12.4 ± 1.8	79
	DBS492/1	N 34°17′56.6″ E 107°04′15.9″	686	28	3.666	1115	11.541	3510	9.227	5142	85.6	57 ± 4	57 ± 4	12.3 ± 1.7	108
Cuihuashan Granite	DBS433/1	N 33°47′33.3″ E 108°51′15.7″	1571	28	0.598	137	3.659	838	8.556	5142	17.7	25 ± 3	27 ± 3	12.7 ± 2.1	44
	DBS430/1	N 33°48′24.1″ E 108°56′29.0″	1177	28	1.403	513	5.592	2045	8.472	5142	86	41 ± 3	41 ± 3	13.5 ± 1.7	97
	DBS428/1	N 33°48′20.8″ E 108°58′07.7″	1083	28	1.84	711	6.86	2650	8.388	5142	95.1	44 ± 3	44 ± 3	13.1 ± 1.7	103
Mishuling Granite	DBS465/1	N 34°01′43.8″ E 105°57′52.1″	1524	17	9.059	1642	21.234	3849	8.556	5142	0	68 ± 5	71 ± 4	12.5 ± 1.5	89
	DBS466/1	N 34°01′35.1″ E 105°57′54.1″	1455	28	11.759	3077	26.166	6847	8.472	5142	0	73 ± 5	74 ± 4	12.4 ± 1.8	101
	DBS467/1	N 34°01′15.6″ E 105°58′17.4″	1382	13	13.218	764	26.263	1518	9.143	5142	4.8	88 ± 7	89 ± 6	11.8 ± 1.8	48
	DBS468/1	N 34°00′23.6″ E 105°59′13.4″	1308	27	7.244	1427	19.087	3760	9.059	5142	1.1	65 ± 4	67 ± 4	12.2 ± 1.6	95
	DBS469/1	N 33°58′34.2″ E 105°59′50.2″	1248	28	7.541	1461	15.964	3093	8.975	5142	65.6	82 ± 5	82 ± 5	12.6 ± 1.6	97
	DBS470/1	N 33°56′58.0″ E 106°00′15.1″	1210	27	4.374	1031	13.151	3100	8.892	5142	84.7	57 ± 4	57 ± 4	12.2 ± 1.6	93
Liuba Granite	DBS483/1	N 33°41′36.2″ E 106°48′05.0″	1613	28	3.486	478	7.796	1069	9.143	5142	100	79 ± 6	79 ± 6	13.7 ± 1.9	105
	DBS481/1	N 33°41′28.3″ E 106°48′35.0″	1484	28	4.54	797	12.103	2109	9.059	5142	11.8	64 ± 5	66 ± 4	12.9 ± 1.7	100
	DBS479/1	N 33°41′15.6″ E 106°49′15.5″	1378	28	3.539	462	7.561	987	8.975	5142	100	81 ± 6	81 ± 6	13.0 ± 1.7	82
	DBS478/1	N 33°41′03.4″ E 106°49′40.9″	1287	28	5.105	703	9.759	1344	8.892	5142	100	90 ± 6	90 ± 6	12.3 ± 1.9	102

(*continued on next page*)

ARTICLE IN PRESS

Table 2 (*continued*)

Rock mass	Sample	Location	Elevation (m)	No. of grains	ρs (10^5/cm^2)	Ns	ρi (10^5/cm^2)	Ni	ρd (10^5/cm^2)	Nd	$P(x^2)$ (%)	Central age (Ma) (±1σ)	Pooled age (Ma) (±1σ)	Mean length (μm) (±1σ)	No. of lengths
	DBS476/1	N 33°41′31.8″ E 106°51′13.2″	1196	28	7.838	1044	19.903	2651	8.808	5142	78	67 ± 4	67 ± 4	12.7 ± 1.9	100
	DBS474/1	N 33°37′19.1″ E 106°54′50.8″	970	28	5.4	817	9.241	1398	8.724	5142	97.1	99 ± 7	99 ± 7	12.8 ± 1.6	86
	DBS472/1	N 33°34′50.6″ E 106°57′11.2″	867	27	10.452	2954	26.213	7408	8.64	5142	9	67 ± 4	67 ± 4	13.0 ± 1.7	86
Foping Granite	DBS455/1	N 33°43′14.7″ E 107°57′57.3″	1688	28	2.788	509	9.839	1796	8.808	5142	18.4	48 ± 4	48 ± 4	12.8 ± 2.3	99
	DBS454/1	N 33°42′52.4″ E 107°57′49.1″	1579	23	7.423	1620	21.258	4639	8.724	5142	84.2	59 ± 4	59 ± 4	12.7 ± 1.8	101
	DBS452/1	N 33°42′02.9″ E 107°56′57.8″	1437	28	15.072	4347	37.346	10771	8.64	5142	0.2	68 ± 4	68 ± 4	12.4 ± 1.7	99
	DBS451/1	N 33°41′32.0″ E 107°56′57.5″	1358	28	2.979	1621	9.346	5086	8.556	5142	11	53 ± 3	53 ± 3	12.6 ± 2.1	107
	DBS449/1	N 33°39′41.9″ E 107°58′06.4″	1224	28	5.381	1746	13.643	4427	8.472	5142	80.3	65 ± 4	65 ± 4	12.3 ± 2.0	107
	DBS446/1	N 33°37′04.4″ E 107°58′22.6″	1074	28	4.66	2279	9.318	4557	8.388	5142	2.6	80 ± 5	81 ± 5	13.3 ± 1.8	104
	DBS444/1	N 33°35′19.3″ E 107°58′48.4″	963	28	5.466	2665	12.599	6143	9.227	5142	7.4	77 ± 5	78 ± 4	13.0 ± 1.9	103
	DBS441/1	N 33°31′47.5″ E 107°59′15.3″	851	28	1.496	750	4.432	2222	9.143	5142	43.8	59 ± 4	60 ± 4	12.5 ± 2.0	105
Ningshan Granite	DBS323/1	N 33°21′24.1″ E 108°26′47.6″	1248	28	3.281	658	13.843	2776	8.64	5142	74.5	40 ± 3	40 ± 3	12.8 ± 1.8	102
	DBS322/1	N 33°20′51.9″ E 108°26′14.4″	1193	27	0.639	145	2.669	606	8.556	5142	73.6	38 ± 4	40 ± 4	12.4 ± 1.6	91
	DBS320/1	N 33°20′07.0″ E 108°26′02.8″	1123	29	5.289	2267	12.187	5223	9.227	5142	0	80 ± 6	80 ± 6	13.4 ± 1.7	106
	DBS319/1	N 33°19′17.3″ E 108°25′49.5″	1074	27	2.596	897	5.739	1983	9.143	5142	9.3	80 ± 6	80 ± 5	12.4 ± 2.0	104
	DBS316/1	N 33°18′46.8″ E 108°24′18.0″	999	28	3.794	1082	13.094	3734	9.059	5142	82.9	51 ± 3	51 ± 3	12.3 ± 1.7	100
	DBS314/1	N 33°21′25.8″ E 108°19′21.7″	831	21	1.688	322	4.688	894	8.957	5142	94.9	63 ± 5	63 ± 5	12.8 ± 1.6	31
Dongjiangkou Granite	DBS426/1	N 33°45′38.0″ E 109°03′30.5″	918	28	5.043	1633	17.137	5549	8.304	5142	88.3	47 ± 3	47 ± 3	12.6 ± 1.9	101
	DBS324/1	N 33°40′04.7″ E 108°38′55.2″	811	28	4.765	1384	19.592	5691	8.22	5142	54.5	39 ± 2	39 ± 2	12.6 ± 2.0	114

Standard track densities (ρd) and induced track densities (ρi) were measured on mica external detectors and fossil track densities (ρs) on internal mica surfaces. Nd, Ns and Ni are the numbers of tracks counted. Ages were calculated using a zeta of 389.4 ± 19.2 (DXB) using Corning CN5 dosimeter glass.

Please cite this article in press as: Chen, H., et al. Apatite fission-track thermochronological constraints on the pattern of late Mesozoic–Cenozoic uplift and exhumation of the Qinling Orogen, central China. Journal of Asian Earth Sciences (2014), http://dx.doi.org/10.1016/j.jseaes.2014.10.004

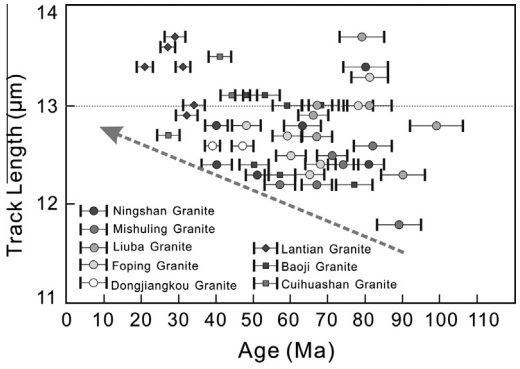

Fig. 4. Age–length relationship schemas for AFT samples of the granites. Ages and track lengths are plotted with an error of 1σ.

we used the method of Donelick et al. (1999). In the modeling, we used the monotonic-variable path setting to allow for both cooling and heating histories. The Kolmogorov–Smirnov test was employed to assess the fit between modeled and measured track-length distributions. For each sample, we obtained 200 good paths and more than 1000 acceptable paths, and up to 20,000 paths were calculated with merit values of 0.5 and 0.05 for good and acceptable fits, respectively. The only exception was for sample DBS483/1, which has no good paths and 4401 acceptable paths.

3.3. Apatite fission-track results and thermal modeling

Apart from three samples (DBS465/1, DBS467/1, and DBS490/1), fission track data for more than 25 apatite grains were able to be obtained from each sample, and the number of measured track lengths was mostly up to 100, ensuring the accuracy of the statistical tests data (Table 2; Donelick et al., 2005). The resulting AFT ages are younger than the timing of magmatic intrusion for all the samples (Tables 1 and 2). Except for a few samples, the χ^2 values for single grain ages in each sample are over 5%, indicating that the sample age is derived from one population of single grain ages and therefore that the AFT ages represent the tectonothermal event. The ages differ among granitic plutons (Table 2), indicating that the Qinling Orogen experienced multiple stages of exhumation (Enkelmann et al., 2006; Hu et al., 2006a). In addition, the relationships between the ages and elevations of samples for each pluton are complex (Fig. 3).

The mean fission-track length (MFTL) of different granitoid plutons varies between 11.8 and 13.7 μm, which indicates differences in the rate of cooling, and the values show a negative correlation with AFT age for all the samples (Fig. 4). Most of the MFTLs for individual samples are shorter than the original track lengths (~14 μm), indicating that most of the samples experienced long-term partial annealing and slow cooling (Donelick et al., 2005; Ketcham et al., 2007; Tagami and Sullivan, 2005). Only a few samples have very high mean track lengths (>13 μm; e.g., DBS421/1 at 13.7 μm), which signify very rapid cooling; this is especially seen in samples of the Lantian Granite.

The modeling results for the eight granitoid plutons studied are shown in turn in Figs. 5–12, and the three colored lines in each figure indicate the best-fit, good, and acceptable paths in the thermal modeling, respectively. Apart from sample DBS483/1, all of the goodness of fit (GOF) values for the modeled ages and modeled lengths of samples are over 0.50, which indicates that the modeling results are statistically significant.

3.3.1. Lantian Granite

The Lantian Granite locates in the S-NCB, which was intruded at Early Cretaceous with the U–Pb age of 133 Ma, and indicated the intra-continental setting of the Qinling Orogen (Fig. 2; Wang et al., 2013). There were two-stage fault deformations nearby the Lantian Granite (Fig. 3a). The southward thrust was prior to the magma intruded, and the northward normal fault overprinted the pluton obviously. Between the two normal faults at north flank of the Lantian Granite, there are six samples were collected between elevations of 990 and 1301 m along transect oriented from the center toward the edge (Fig. 3a).

The AFT central ages range from 21 to 34 Ma (Table 2). The ages generally decrease from the edge to the center of the massif, although the samples from the northern and southern edges of the massif have the lowest and highest elevations, which have the oldest ages of 32 and 34 Ma, respectively (Fig. 3a). Apart from sample DBS418/1, the AFT ages of the samples cover a small age range of about 7 Ma, which indicates that the Lantian Granite was uplifted rapidly. The mean track lengths of all six samples range from 12.9 to 13.7 μm with standard deviations of between 1.5 and 2.2 μm. Most of the track lengths are over 13 μm, indicating that the granite experienced rapid cooling, supporting the interpretation of the AFT ages.

The modeling paths of these six samples can be divided into three groups, and the initial timings and the stages of cooling differ among the groups (Fig. 5). Two samples (DBS417/1 and DBS422/1) have the same features of modeled *T*–*t* paths. The rapid cooling of this group of samples started at ~50 Ma and the oldest modeled age (means the samples uplift into the PAZ) for this group is ~40 Ma, and prolonged cooling to the upper part of the PAZ (~80 °C) at 31.5 Ma with the rapid cooling rate at ~3 °C/m.y. Subsequently, the granite entered a stage of slow cooling rate at ~1 °C/m.y. between 30 and 10 Ma. The characteristics of samples DBS419/1, DBS420/1 and DBS421/1 of modeled *T*–*t* paths also show two stages of cooling. For this group, the initiation of cooling occurred at ~40 Ma and the oldest modeled age is 35 Ma, which is a little later than in the first group of samples. This rapid cooling history ended at about 25 Ma on the temperature of 60 °C representing the top of the PAZ with the cooling rate at ~3 °C/m.y. The youngest sample (DBS418/1) shows two stages of cooling. The initial cooling occurred at ~30 Ma and prolonged to 20 Ma with a rapid cooling rate at ~3 °C/m.y., which is the youngest age of the Lantian Granite. A second stage of cooling started at ~20 Ma, with a cooling rate of ~2 °C/m.y. lower than that of the first stage.

Similar to the age-elevation characteristics of Fig. 3a, the AFT data for the Lantian Granite do not appear to show a standard age-altitude pattern where the oldest observed ages are found at the highest locations. Because the cooling age is obviously later than the crystallization age of the Lantian Granite, and the rock cooling was from its edge to its center between 50 and 25 Ma, this rapid cooling at ~3 °C/m.y. maybe related with the exhumation and erosion. Subsequently, the Lantian Granite underwent slow cooling at ~1 °C/m.y., and leading to the youngest sample (DBS418/1) being uplifted close to the highest location with a rapid cooling rate at ~3 °C/m.y., this rock cooling was considered to relate with the movement on normal faults. The thermal modeling and AFT ages revealed the Lantian Granite experience the early rapid cooling at ~3 °C/m.y. by the exhumation, and underwent a slow cooling at ~1 °C/m.y. by the uplift on the normal fault.

3.3.2. Baoji Granite

Baoji Granite locates at the northern of NQB, which was intruded at Late Triassic with the U–Pb age of 217 Ma in the post-collision setting of the Qinling Orogen (Fig. 2; Lu et al., 1999). Baoji Granite underwent the southward thrust at early and later northward normal fault (Fig. 3b). The thrust developed in the pluton and Proterozoic strata, and the normal fault superposed on the Cretaceous and Cenozoic strata (Fig. 3b). Seven

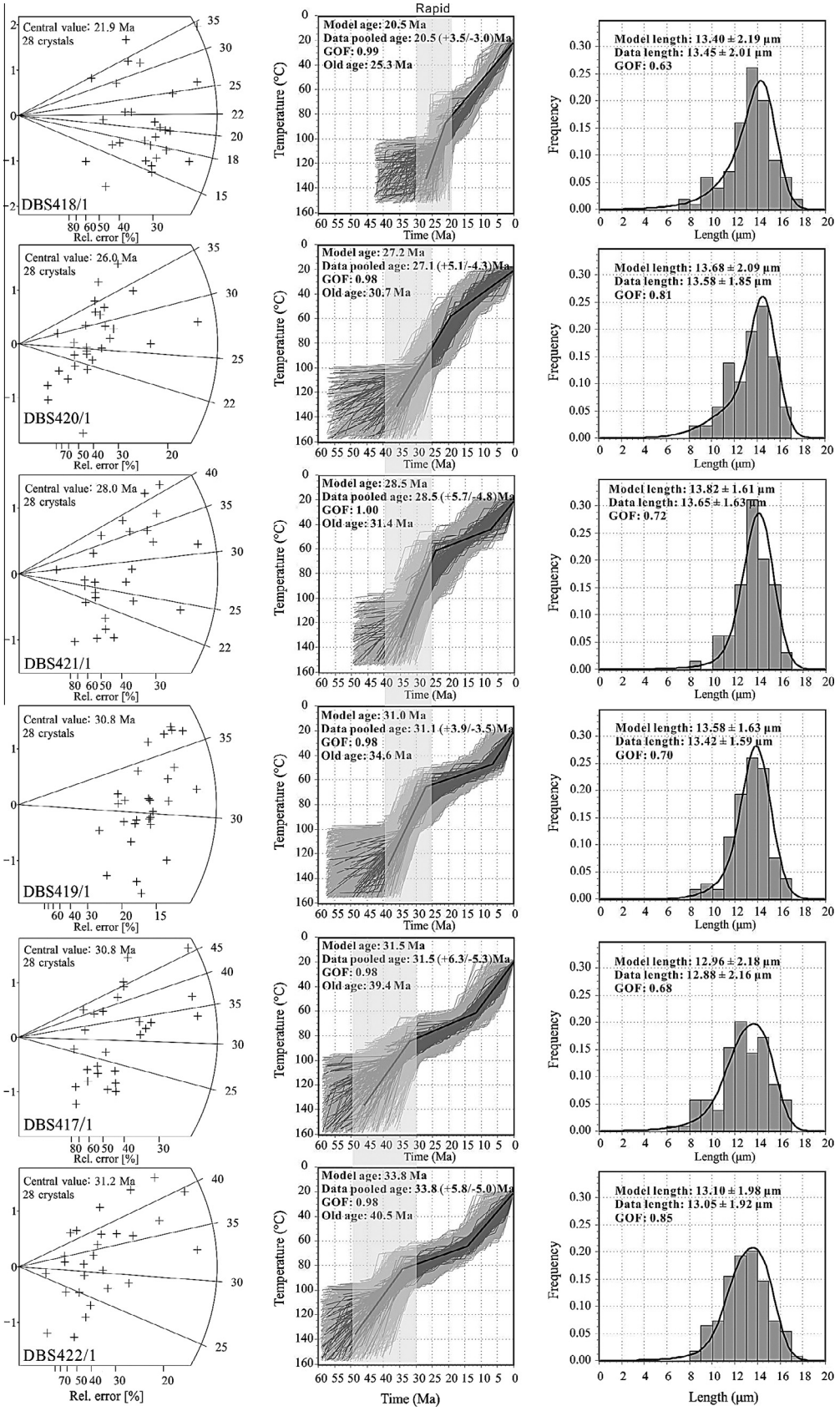

Fig. 5. HeFTy-based thermal history models: radial plots of the central age (left), temperature–time paths (center), and *c*-axis projected confined fission-track length distributions (right) of the Lantian Granite in the S-NCB. In the temperature–time path graphs, the grayish lines represent the acceptable paths, the charcoal-gray lines are good paths, and the black bold line is the best-fitting path. The modeled and pooled ages (with 1σ error) are shown in the time–temperature history graphs; the measured and modeled track lengths (with 1σ error) are shown in the track length distribution diagram; and the GOF values are listed in the graphs. The dark-gray shading depicts relatively rapid cooling (>1 °C/my) that occurred during three stages at 50–30, 40–25, and 30–20 Ma, respectively.

Please cite this article in press as: Chen, H., et al. Apatite fission-track thermochronological constraints on the pattern of late Mesozoic–Cenozoic uplift and exhumation of the Qinling Orogen, central China. Journal of Asian Earth Sciences (2014), http://dx.doi.org/10.1016/j.jseaes.2014.10.004

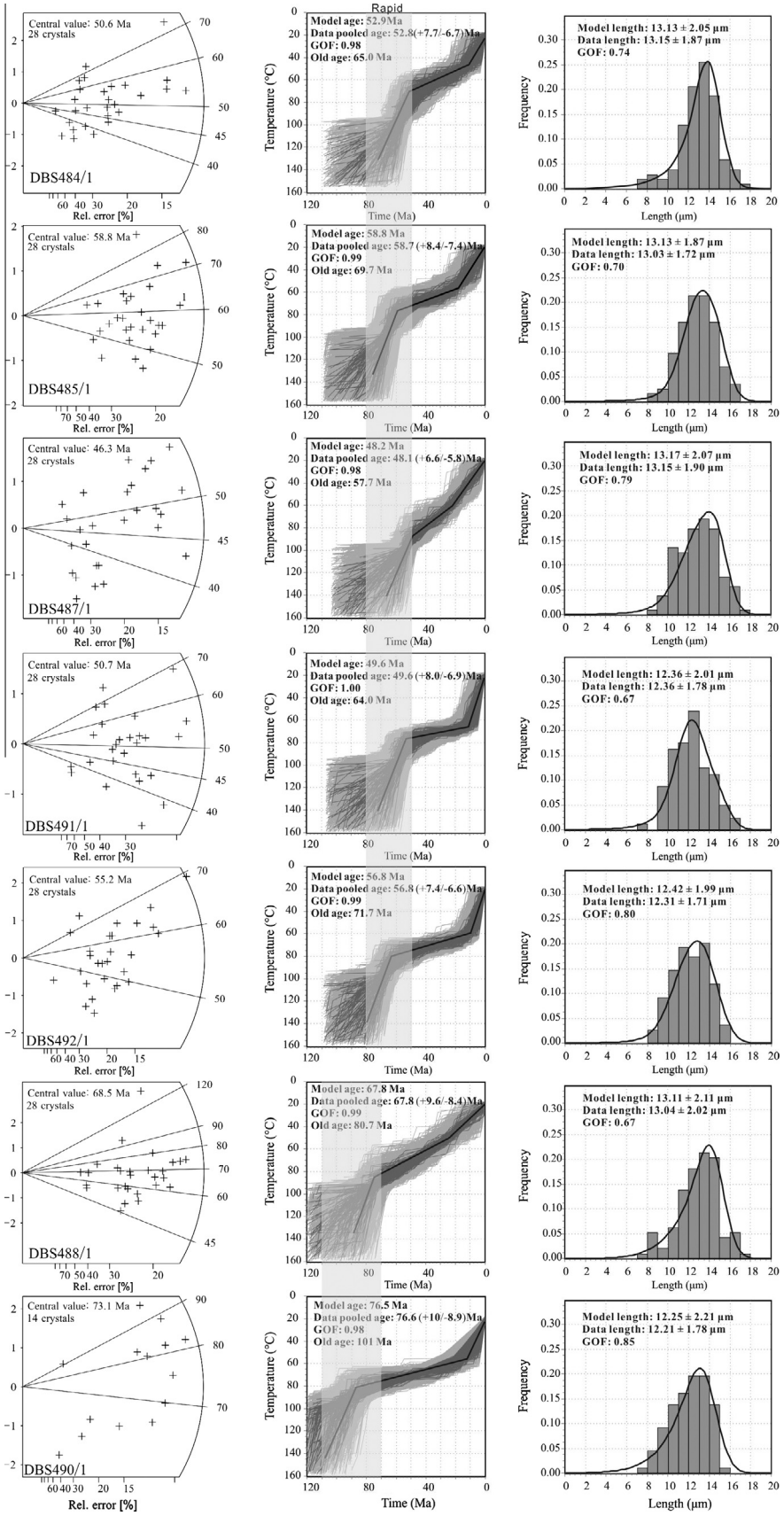

Fig. 6. HeFTy-based thermal history models: radial plots of the central age (left), temperature–time paths (center), and *c*-axis projected confined fission-track length distributions (right) of the Baoji Granite in the NQB. The symbols and notation are the same as in Fig. 5. The dark-gray shading depicts relatively rapid cooling that occurred during two stages at 110–70 and 80–50 Ma.

Please cite this article in press as: Chen, H., et al. Apatite fission-track thermochronological constraints on the pattern of late Mesozoic–Cenozoic uplift and exhumation of the Qinling Orogen, central China. Journal of Asian Earth Sciences (2014), http://dx.doi.org/10.1016/j.jseaes.2014.10.004

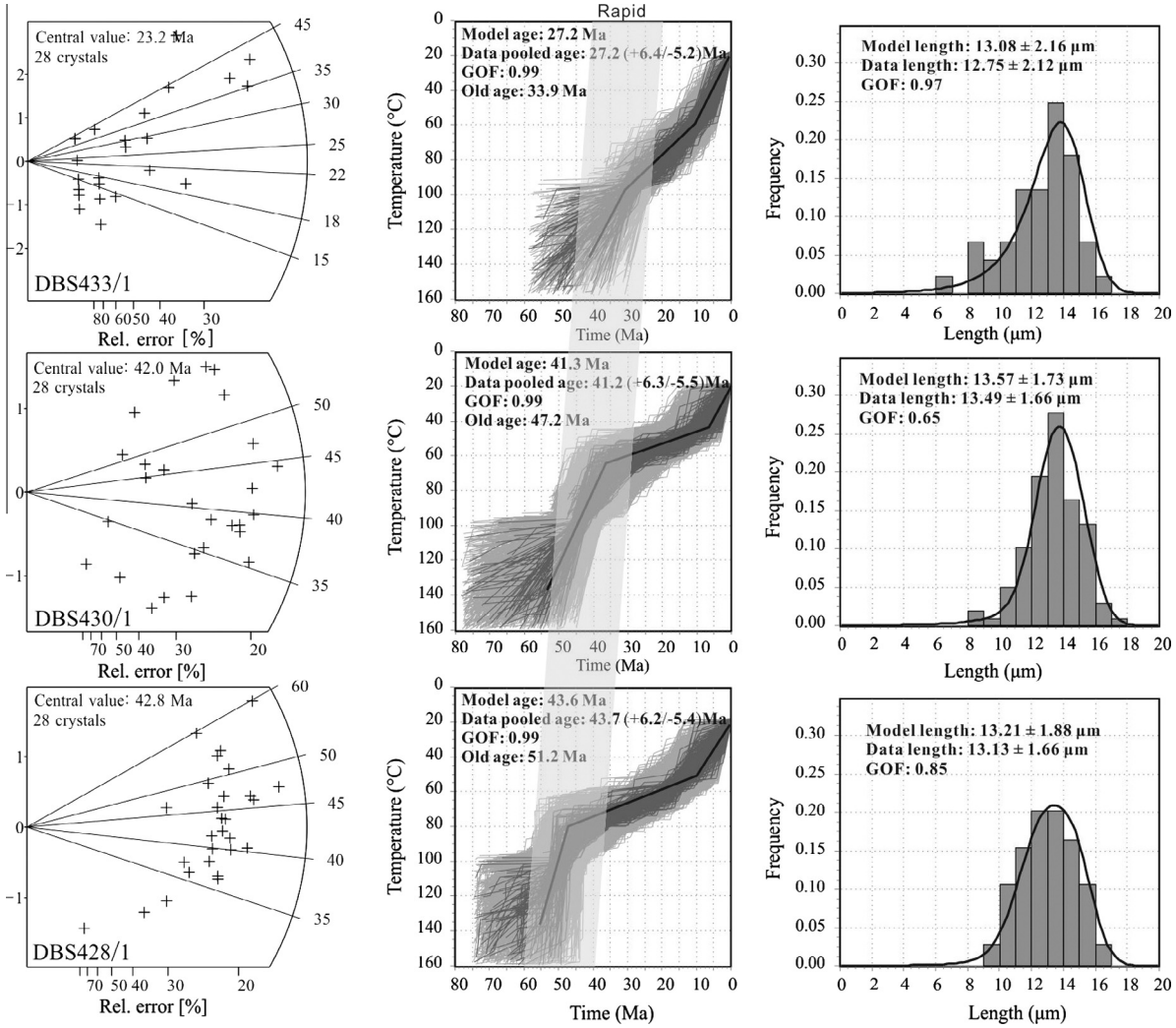

Fig. 7. HeFTy-based thermal history models: radial plots of the central age (left), temperature–time paths (center), and *c*-axis projected confined fission-track length distributions (right) of the Cuihuashan Granite in the NQB. The symbols and notation are the same as in Fig. 5. The dark-gray shading depicts relatively rapid cooling that occurred from west to east during 60 to 25 Ma.

samples were collected between 686 and 1521 m elevation along transect among these two faults (Fig. 3b).

The AFT central ages range from 44 to 77 Ma and can be divided into two groups (Fig. 3b). The four lower-elevation samples show an increase in age with elevation from 50 to 77 Ma, and the three higher-elevation samples range in age between 48 and 59 Ma, which indicates another cooling stage since ~60 Ma. The mean track lengths of these seven samples range from 12.2 to 13.1 μm with standard deviations of between 1.7 and 2.0 μm. The lengths can also be divided into two groups similar to those of the age data. The track lengths of the three higher-elevation samples are over 13 μm, which indicates rapid cooling, and the three lower-elevation samples have lengths of <13 μm and are mainly between 12.2 and 12.4 μm, which indicates a slow cooling.

The modeling results for the Baoji Granite can be divided into two groups of samples. Five samples are modeled as having a similar cooling path, suggesting that rapid cooling to the position of the upper PAZ (temperatures of 70–80 °C) occurred between 80 and 50 Ma with cooling rate at ~2 °C/m.y. (Fig. 6), and the oldest modeled age is 71.7 Ma. Subsequently, the granitoid pluton underwent slow cooling to reach the top of the PAZ (~60 °C) at ~0.3 °C/m.y. prolonged to 20 Ma. For the other two samples, DBS488/1 and DBS490/1, the cooling occurred earlier, starting at ~110 Ma, and the oldest modeled age is 101 Ma (Fig. 6). This group of samples was cooling to the position of the upper PAZ (~80 °C) through to 70 Ma with cooling rate at ~1.5 °C/m.y. Subsequently, the samples entered a stage of slow cooling at ~0.4 °C/m.y. that continued for 50 Ma.

Overall, the Baoji Granite experienced two stages of cooling. The first stage was one of rapid cooling that took place between 110 and 50 Ma, during which the temperature of the samples cooled from the bottom of the PAZ to the upper part of the PAZ (70–80 °C) at ~1.5–2.0 °C/m.y. This stage can be divided into two phases: the initial cooling was from 110 to 80 Ma, and the later one was from 70 to 50 Ma (Fig. 3b). The second stage was slow cooling to the top of the PAZ (60 °C) between 50 and 20 Ma at rate of ~0.3–0.4 °C/m.y. In contrast to the age-elevation pattern (Fig. 3b), the initial rapid cooling was recorded on the lower elevation samples (e.g. DBS488/1 and DBS490/1), and also underwent the slow cooling. The spatial relationship of the samples and faults show that the samples located at the north of the thrust fault and south of the normal fault, and the faults superposed on different units. We considered that the Baoji Granite underwent slow cooling affected with the normal fault after the earlier rapid cooling, and the rapid cooling may be related to the uplift induced by the thrust.

Please cite this article in press as: Chen, H., et al. Apatite fission-track thermochronological constraints on the pattern of late Mesozoic–Cenozoic uplift and exhumation of the Qinling Orogen, central China. Journal of Asian Earth Sciences (2014), http://dx.doi.org/10.1016/j.jseaes.2014.10.004

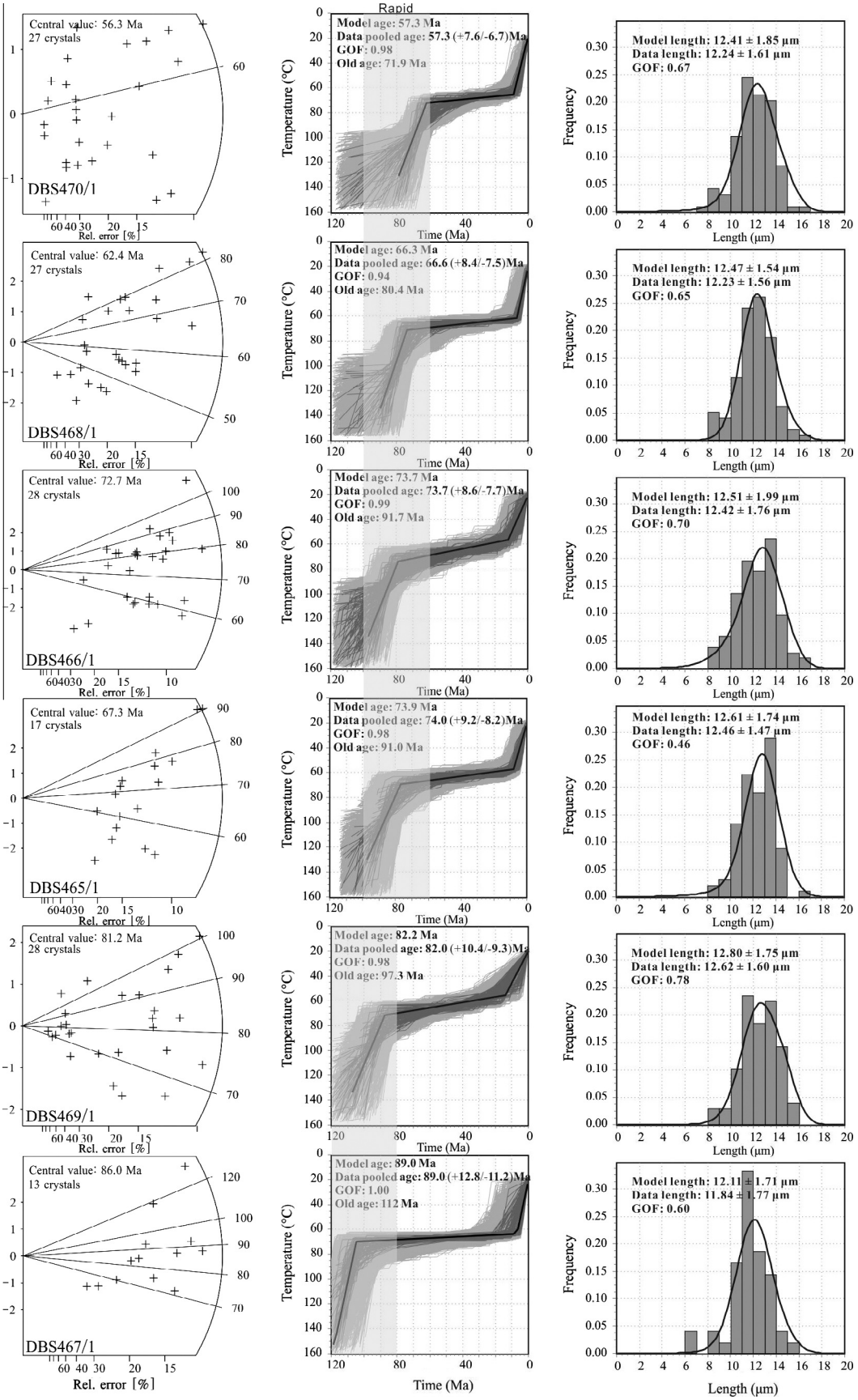

Fig. 8. HeFTy-based thermal history models: radial plots of the central age (left), temperature–time paths (center), and *c*-axis projected confined fission-track length distributions (right) of the Mishuling Granite in the SQB. The symbols and notation are the same as in Fig. 5. The dark-gray shading depicts relatively rapid cooling that occurred during two stages at 120–80 and 110–60 Ma.

Please cite this article in press as: Chen, H., et al. Apatite fission-track thermochronological constraints on the pattern of late Mesozoic–Cenozoic uplift and exhumation of the Qinling Orogen, central China. Journal of Asian Earth Sciences (2014), http://dx.doi.org/10.1016/j.jseaes.2014.10.004

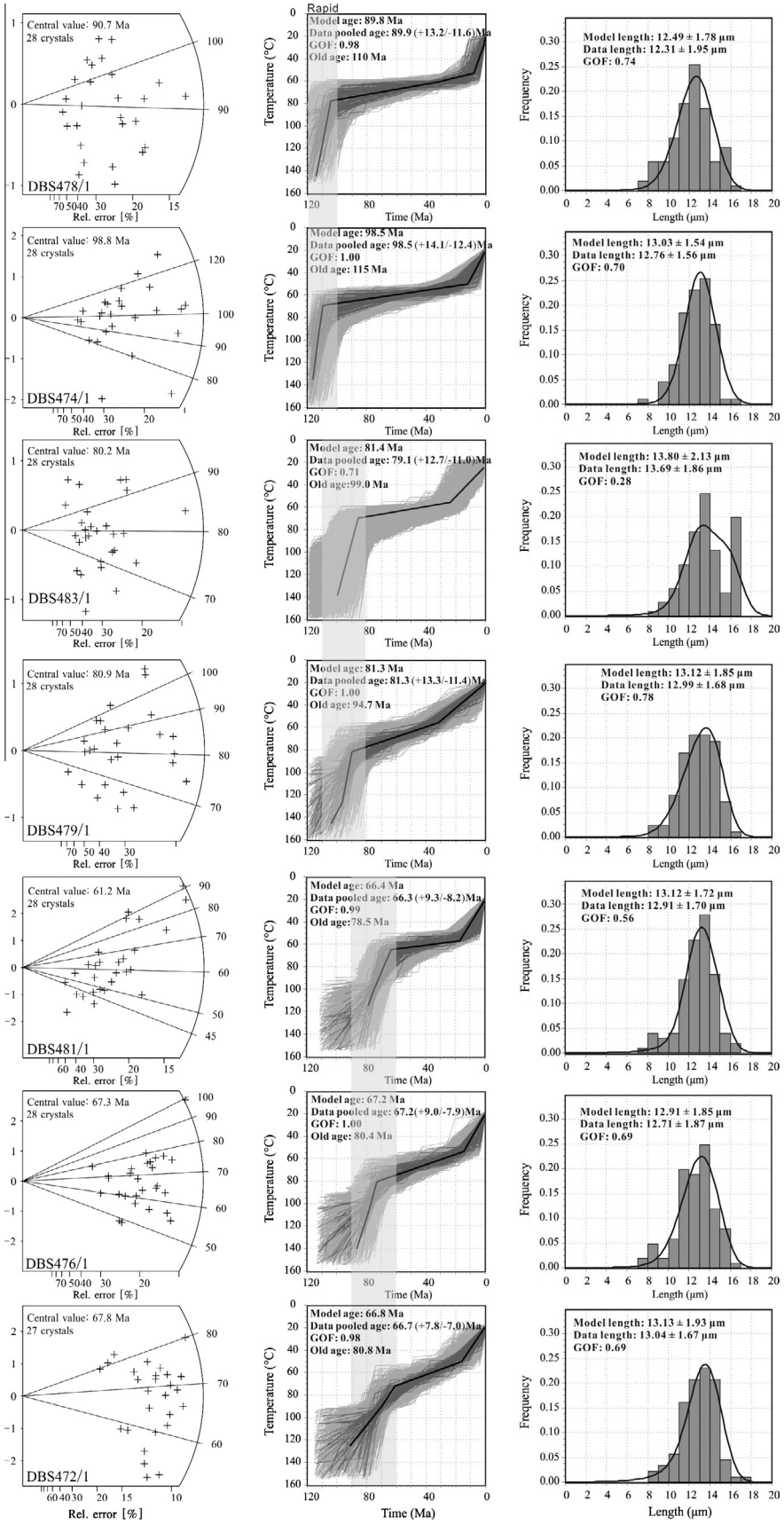

Fig. 9. HeFTy-based thermal history models: radial plots of the central age (left), temperature–time paths (center), and *c*-axis projected confined fission-track length distributions (right) of the Liuba Granite in the SQB. The symbols and notation are the same as in Fig. 5. The dark-gray shading depicts relatively rapid cooling that occurred during three stages at 120–100, 110–80, and 90–60 Ma.

Please cite this article in press as: Chen, H., et al. Apatite fission-track thermochronological constraints on the pattern of late Mesozoic–Cenozoic uplift and exhumation of the Qinling Orogen, central China. Journal of Asian Earth Sciences (2014), http://dx.doi.org/10.1016/j.jseaes.2014.10.004

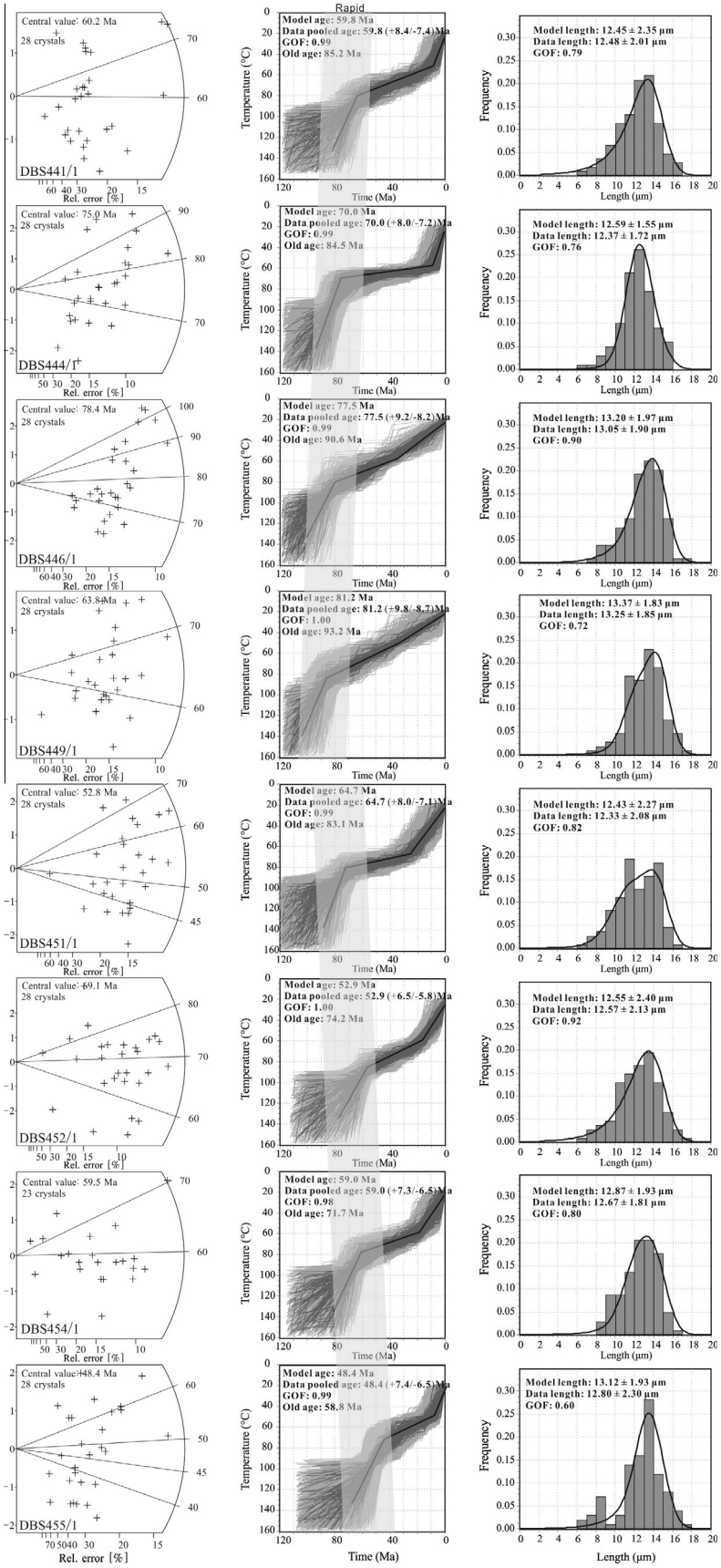

Fig. 10. HeFTy-based thermal history models: radial plots of the central age (left), temperature–time paths (center), and *c*-axis projected confined fission-track length distributions (right) of the Foping Granite in the SQB. The symbols and notation are the same as in Fig. 5. The dark-gray shading depicts relatively rapid cooling that occurred during two stages at 110–60 and 90–40 Ma.

Please cite this article in press as: Chen, H., et al. Apatite fission-track thermochronological constraints on the pattern of late Mesozoic–Cenozoic uplift and exhumation of the Qinling Orogen, central China. Journal of Asian Earth Sciences (2014), http://dx.doi.org/10.1016/j.jseaes.2014.10.004

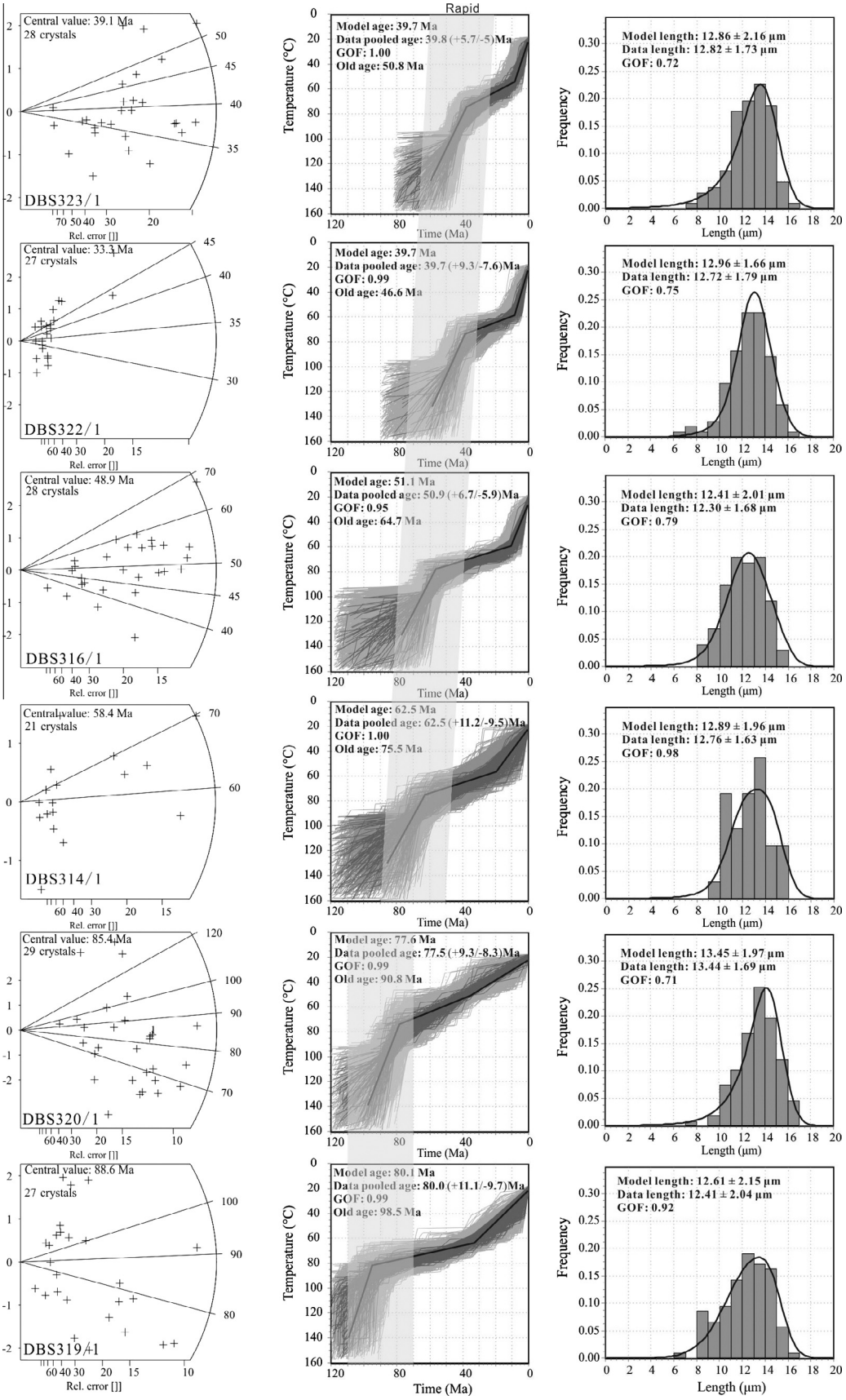

Fig. 11. HeFTy-based thermal history models: radial plots of the central age (left), temperature–time paths (center), and *c*-axis projected confined fission-track length distributions (right) of the Ningshan Granite in the SQB. The symbols and notation are the same as in Fig. 5. The dark-gray shading depicts relatively rapid cooling that occurred during two stages at 110–70 and 90–30 Ma.

Please cite this article in press as: Chen, H., et al. Apatite fission-track thermochronological constraints on the pattern of late Mesozoic–Cenozoic uplift and exhumation of the Qinling Orogen, central China. Journal of Asian Earth Sciences (2014), http://dx.doi.org/10.1016/j.jseaes.2014.10.004

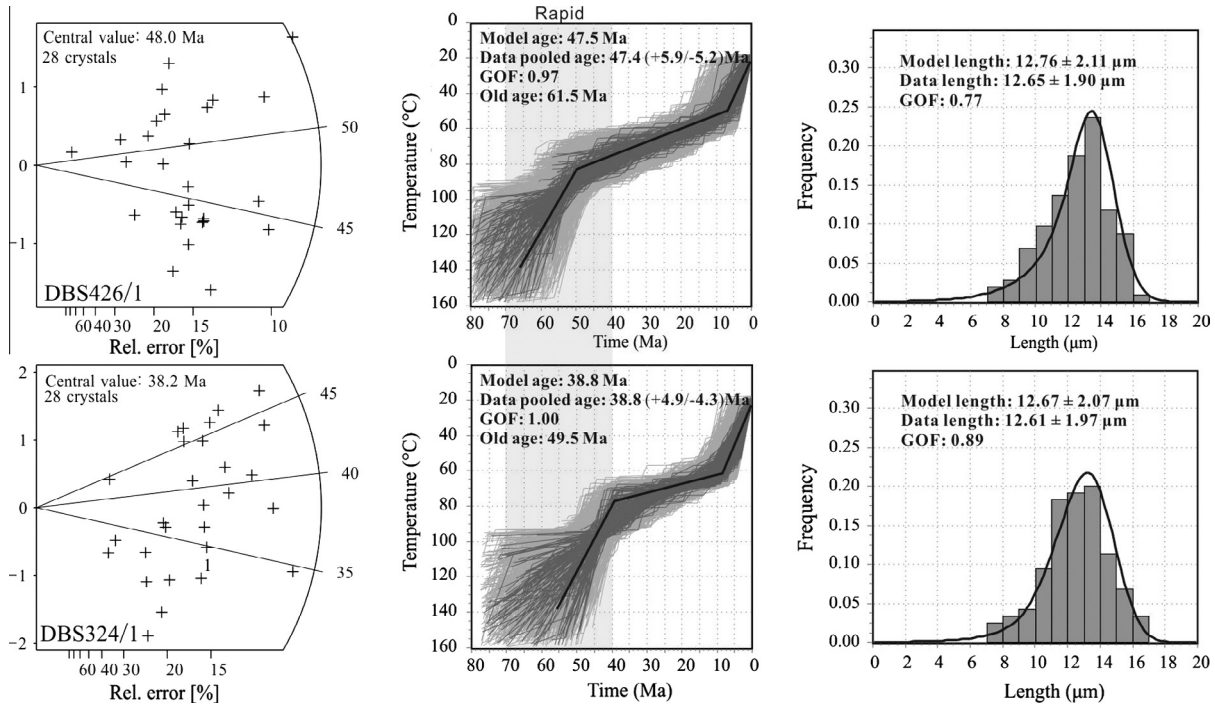

Fig. 12. HeFTy-based thermal history models: radial plots of the central age (left), temperature–time paths (center), and *c*-axis projected confined fission-track length distributions (right) of the Dongjiangkou Granite in the SQB. The symbols and notation are the same as in Fig. 5. The dark-gray shading depicts relatively rapid cooling that occurred from 70 to 40 Ma.

3.3.3. Cuihuashan Granite

Cuihuashan Granite locates in the eastern NQB, and also parallel to the fault separating the NQB and the SQB. The U–Pb age of the granite is 227 Ma, and intruded in the post-collision setting of Qinling Orogen (Jiang et al., 2010). Three samples were collected between 1083 and 1571 m elevation parallel to the long axis of the Cuihuashan Granite at the north of the sinistral fault (Fig. 3c).

The central ages decrease with increasing elevation from 44 to 25 Ma, and can be divided into two groups. Sample DBS433/1 in the west is younger and has shorter track lengths (<12.7 μm) than the samples in the east (track lengths > 13 μm), which indicates that sample DBS433/1 underwent a different cooling path to the eastern samples.

The modeling results for the Cuihuashan Granite show that the eastern part of the pluton was cooled earlier than the western part (Fig. 7). Sample DBS428/1 in the eastern part was cooling rapidly at 55 Ma and reached the mid-upper PAZ (80 °C) at ~50 Ma on rate of ~5 °C/m.y., and the oldest modeled age is 51.2 Ma. And another slow cooling stage continued for approximately 30 Ma at ~0.7 °C/m.y. after the rapid cooling to reach 60 °C at 20 Ma. The initiation of uplift of sample DBS430/1 in the middle of the transect is similar to that of DBS428/1, and the oldest modeled age is 47.2 Ma, but the sample remained in the rapid cooling stage with slower rate at ~4 °C/m.y. for longer and reached the top of the PAZ (60 °C) at 35 Ma. The westernmost sample (DBS433/1) started to be cooled at ~40 Ma at ~3 °C/m.y., and underwent a stage of stable cooling with a slightly slower cooling rate of ~2 °C/m.y. between 30 and 10 Ma, and the oldest modeled age is 33.9 Ma.

This east–west difference in the results of the modeling is consistent with the age-elevation pattern (Fig. 3c), and indicates that the Cuihuashan Granite was cooled rapidly and propagated from east to west. Because the sample distribution is parallel to the sinistral movement of the boundary fault, which indicate the cooling of the Cuihuashan Granite is able to reveal the characteristics of uplift and deformation along the fault during the Cenozoic.

3.3.4. Mishuling Granite

Mishuling Granite intruded at 213 Ma in the post-collision stage in the western SQB (Qin et al., 2009). And the western SQB underwent the multi-stage thrust deformation before and after the Mishuling Granite intruded, and the later thrust faults were covered by the Neogene strata (Fig. 3d). Six samples were collected between 1210 and 1524 m elevation along transect crossing the Mishuling Granite (Fig. 3d).

The AFT central ages range from 57 to 89 Ma and generally increase with elevation. However, the oldest observed ages in the middle samples rather than in the highest-elevation sample, and the ages also decrease from the center to the edge of the pluton. The mean track lengths of these six samples range from 11.8 to 12.6 μm with standard deviations of between 1.5 and 1.8 μm, indicating slow cooling.

The modeling paths and uplift times for these six samples are essentially consistent with each another (Fig. 8). Four samples (i.e. DBS465/1, DBS466/1, DBS468/1 and DBS470/1) show that rapid cooling began at ~100 Ma with cooling rate at ~3 °C/m.y., and the oldest modeled age is 91.7 Ma. The other two samples (i.e. DBS467/1 and DBS469/1) started cooling earlier, at ~120 Ma, the cooling rate is ~6 °C/m.y. and the oldest modeled age is 112 Ma. All of the thermal modeling reveals that the Mishuling Granite reached the top of the PAZ (~60 °C) at ~60 Ma, and then entered a stable stage with the cooling rate at 0.2 °C/m.y.

The geological feature of the Mishuling Granite indicated that the granitic pluton experienced the thrust deformation before Neogene. The spatial relationship between the samples and faults indicate the rapid cooling was related to the thrust deformation, especially for the earliest cooling of the DBS467/1 and DBS469/1, which were nearby and separated by the thrust fault. And the upper hanging sample (DBS467/1) is earlier than the lower sample (DBS469/1) (Fig. 8). The uniformity thermal modeling data for each sample and geological tectonic framework indicate the rapid cooling of the Mishuling Granite ranged from ~120 Ma to 60 Ma with

Please cite this article in press as: Chen, H., et al. Apatite fission-track thermochronological constraints on the pattern of late Mesozoic–Cenozoic uplift and exhumation of the Qinling Orogen, central China. Journal of Asian Earth Sciences (2014), http://dx.doi.org/10.1016/j.jseaes.2014.10.004

cooling rate at ~3–6 °C/m.y. was related to the uplift induced by the thrust deformation. And the thrust deformation has ended since ~60 Ma, which was revealed by the slowly cooling at 0.2 °C/m.y. of Mishuling Granite (Fig. 8).

3.3.5. Liuba Granite

The Liuba Granite intruded in the post-collision setting with U–Pb age of 218 Ma in the Qinling Orogen (Zhang et al., 2006), which consists of a series of subplutons at the surface, and the host rock consists of Paleozoic strata. The Liuba Granite experienced the later thrust deformation southward or northward (Fig. 3e). Seven AFT samples were collected between 867 and 1613 m elevation along transect that crossed two subplutons, which was separated by a southward thrust fault (Fig. 3e).

The central ages can be divided into two groups: the first group (i.e. DBS472/1, DBS476/1 and DBS481/1) has central ages of <70 Ma that are clustered between 64 and 67 Ma, the second group (i.e. DBS474/1, DBS478/1, DBS479/1 and DBS483/1) has central ages of >80 Ma. The ages generally decrease with elevation, indicating that the uplift of the pluton was influenced by an adjacent thrust fault (Fig. 3e). The mean track lengths of all seven samples range from 12.3 to 13.7 μm with standard deviations of 1.6–1.9 μm.

Apart from one sample (DBS483/1) that did not have a best-fit curve, the cooling of the Liuba Granite can be divided into three stages (Fig. 9). The earliest cooling occurred at 120–100 Ma with the cooling rate of ~3 °C/m.y., as indicated by samples DBS474/1 and DBS478/1, and the oldest modeled age is 115 Ma. The next cooling stage occurred from 110 to 80 Ma at ~2 °C/m.y., as modeled from samples DBS483/1 and DBS479/1, with the oldest modeled age being 99 Ma. These four samples show continuous cooling but a nonstandard age-altitude pattern in which the oldest observed ages are found at the highest elevations, which may be related to later thrust faulting in the Liuba Granite, and the rapid cooling was affected by uplift with the thrust deformation. There also experienced a slow cooling at ~0.15 °C/m.y. from 80 to 20 Ma, which indicated the Liuba Granite was turned into a stable stage. The most recent rapid cooling occurred between 90 and 60 Ma with the cooling rate of ~2.5 °C/m.y., as shown by samples DBS472/1, DBS476/1 and DBS481/1, and the oldest modeled age is 80.8 Ma (Fig. 9), and also experienced slow cooling from 60 to 20 Ma. These three samples are located at different location of the granitic pluton, and other location was in a stable stage at the same time, which indicated the pluton was cooled by exhumation but not the tectonic influence.

3.3.6. Foping Granite

The Foping Granite is located in the central of the Foping Dome in the SQB at Early Mesozoic, the crystallization age is 212–217 Ma on U–Pb dating (Dong et al., 2012; Qin et al., 2008; Zhang et al., 2001), and was intruded into Paleozoic strata in the post-collision setting in Qinling Orogen (Fig. 3f). The Foping Granite obviously experienced the earlier detachment deformation in dome center and later thrust outward (Fig. 3f). Eight samples were collected between 851 and 1688 m elevation along a transect that crossed the Foping Dome, with four granodioritic samples of these samples being obtained to the north.

The central ages of these samples can be divided into two groups. The first group comprises the three lower-elevation samples (i.e. DBS441/1, DBS444/1, and DBS446/1), who's ages generally increase with elevation from 59 to 81 Ma. The mean track lengths of these three samples range from 12.5 to 13.3 μm with standard deviations of between 1.8 and 2.0 μm, indicates rapid cooling. The second group comprises the five higher-elevation samples (i.e. DBS449/1, DBS451/1, DBS452/1, DBS454/1 and DBS455/1), whose age decrease with elevation from 68 to 48 Ma. The mean track lengths of these five samples range from 12.3 to 12.8 μm with standard deviations of between 1.7 and 2.3 μm, which indicates a slower cooling history than that of the first group. These two groups of samples are separated by a detachment fault (Fig. 3f), and the second group is higher in elevation than the first group, which indicates that the Foping Granite underwent two stages of cooling associated with faulting deformation.

Thermal modeling of these eight samples also reveals two stages of cooling related to the age-elevation feature (Fig. 10). The first group (comprising the four lowest-elevation samples; namely, DBS441/1, DBS444/1, DBS446/1, and DBS449/1) was cooling rapidly from 100 to 60 Ma at rate of ~2.5 °C/m.y., and the oldest modeled age is 93.2 Ma from sample DBS449/1 (the sample with the highest elevation of this group). These four samples are surrounded by the detachment faults and are also located at the center of the Foping Dome, which indicates that the first stage of cooling was related to the uplift of the dome. This rapid cooling was continued by a slow cooling at ~0.3 °C/m.y. from 60 to 10 Ma. The second group was cooling from 90 to 40 Ma at rate of ~1 °C/m.y. as modeled on the four higher-elevation samples (DBS451/1, DBS452/1, DBS454/1, and DBS455/1), which are located in the northern part of the Foping Dome. These four samples reveal a nonstandard age-elevation pattern, with the youngest sample at the highest location, which indicates that the later cooling may have been caused by thrust deformation of the pluton (Fig. 3f). And the following cooling is at a slow cooling rate of ~0.5 °C/m.y., which was faster than the first group. This difference indicates the thrust fault at north of the Foping Granite also affected the slow cooling in Cenozoic.

3.3.7. Ningshan Granite

Ningshan Granite locates at east of the Foping Granite in the middle SQB, the U–Pb age of the pluton is 210 Ma, and intruded in the post-collision setting (Jiang et al., 2010). The Ningshan Granite also underwent a detachment deformation same as the Foping Granite, and superposed the later NE–SW trending sinistral strike-slip deformation. Five samples were collected between 999 m and 1248 m elevation along transect from the bottom of the Ningshan Granite, and sample DBS314/1 was collected nearby the transect with low elevation of 831 m (Fig. 3g).

The central ages can be divided into two groups. The two samples (i.e. DBS319/1 and DBS320/1) of the first group have the same age of 80 ± 6 Ma, and the mean track lengths of these two samples are 12.4 and 13.4 μm, with standard deviations of 2.0 and 1.7 μm, respectively, which indicate rapid cooling. The ages of the second group (i.e. DBS314/1, DBS316/1, DBS322/1 and DBS323/1) decrease with elevation from 63 to 38 Ma, and the mean track lengths of these four samples range from 12.3 to 12.8 μm with standard deviations of between 1.6 and 1.8 μm, which indicates the slow cooling.

The modeling results for these six samples show two phases of cooling (Fig. 11). The results obtained for the samples from the middle elevations (i.e. DBS319/1 and DBS320/1) of the transect reveal that the earlier cooling occurred at 110–80 Ma at cooling rate of ~1.5 °C/m.y. to the upper PAZ (~80 °C), and the oldest modeled age is 98.5 Ma. The samples from the lowest elevations (i.e. DBS314/1 and DBS316/1) and highest elevations (i.e. DBS322/1 and DBS323/1) experienced continuous cooling from 80 to 40 Ma at ~1 °C/m.y., and the oldest modeled age is 75.5 Ma. However, the age-elevation pattern is not standard, and the sample with the youngest age is found at the highest elevation, which indicates that the later stage of cooling may have been a result of sinistral deformation. For the earlier cooling stage, the rate of the cooling is faster than the later stage, which may be related to the detachment based on the deformation sequence.

Please cite this article in press as: Chen, H., et al. Apatite fission-track thermochronological constraints on the pattern of late Mesozoic–Cenozoic uplift and exhumation of the Qinling Orogen, central China. Journal of Asian Earth Sciences (2014), http://dx.doi.org/10.1016/j.jseaes.2014.10.004

3.3.8. Dongjiangkou Granite

The Dongjiangkou Granite with east–west trending axis is located on the northern margin of the SQB, and nearby to the boundary sinistral fault. The U–Pb age of the pluton is 218–219 Ma, and intruded in the post-collision setting (Jiang et al., 2010; Yang et al., 2009). One sample was collected from each of the western and eastern sides of the Dongjiangkou Granite at elevations of 811 (DBS324/1) and 918 m (DBS426/1), respectively.

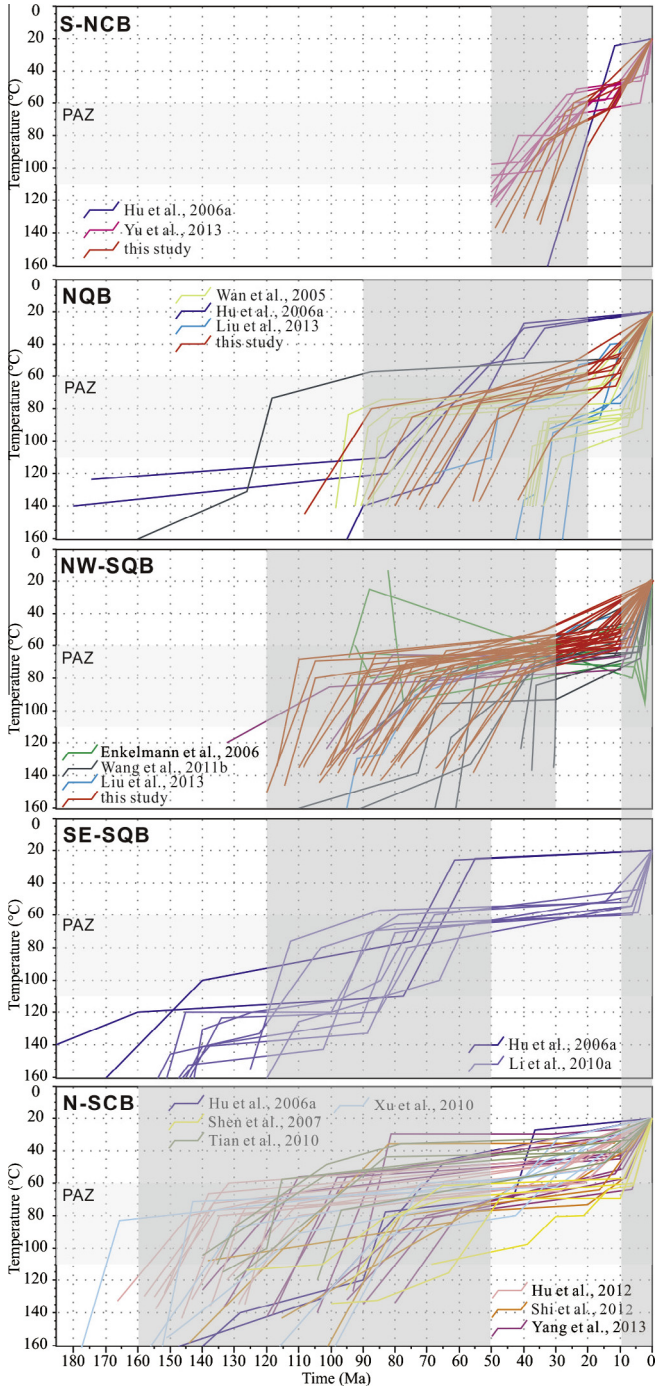

Fig. 13. Temperature–time statistics of AFT modeling data of the present study and of previous studies for five micro-blocks (S-NCB, NQB, NW-SQB, SE-SQB, and N-SCB) of the Qinling Orogen. The light-gray shading and 'PAZ' represent the partial annealing zone; the dark-gray shading depicts relatively rapid cooling for each micro-block, which occurred during four stages at 160–120, 120–90, 90–50, and 50–20 Ma.

The AFT central ages are 39 and 47 Ma, respectively (Fig. 3h). The mean track length for both samples is 12.6 μm with standard deviations of 2.0 and 1.9 μm, respectively, which indicates slow cooling.

The modeling of these two samples yielded consistent results, revealing that rapid cooling occurred from 70 to 40 Ma at cooling rate of ~1.5 °C/m.y. (Fig. 12), and following with a slow cooling at ~0.6 °C/m.y. prolonged to 10 Ma. Although there are only two samples for this granite, the eastern sample (DBS426/1) was cooled earlier than the western sample (DBS324/1). The eastern sample indicates that rapid cooling occurred at 70–50 Ma compared with 55–40 Ma for the western sample, and the oldest modeled ages are 61.5 and 49.5 Ma, respectively. The long axis of the granite was also parallel to the fault, and the cooling from east to west indicated the cooling related to the sinistral deformation nearby the granite. This rapid cooling occurred later than other parts of the SQB (e.g. Mishuling and Foping Granites).

3.3.9. Summary

On the basis of the new AFT ages and *T–t* modeling of 45 Mesozoic granite samples from the eight studied plutons in the S-NCB, NQB, and SQB, we confirm that the Qinling Orogen began to be cooling induced by the thrust and detachment deformation during the late Early Cretaceous at the latest, and that it subsequently experienced three periods of rapid cooling at 120–90, 90–50, and 50–20 Ma (Figs. 5–12). The cooling histories related to the geological background are different for individual plutons and micro-blocks.

The first period of rapid cooling (120–90 Ma) occurred mainly in the SQB with cooling rate of 1.5–6 °C/m.y., and the cooling occurred earlier in the west than in the east during the Late Cretaceous. The earliest cooling with thrust deformation in this period occurred at ~120 Ma, in the western granites, such as the Mishuling and Liuba Granites, and then propagated to the Foping and Ningshan Granites on detachment deformation in the east and the Baoji Granite on thrust deformation in the north.

The second period of rapid cooling (90–50 Ma) at 1–2.5 °C/m.y. associated with the faulting deformation and exhumation occurred mainly in the SQB and NQB. This cooling history also propagated from west to east, as shown by the rapid cooling of the Liuba Granite and Dongjiangkou Granite on the exhumation condition. Moreover, the rapid cooling of the Baoji Granite in the western NQB occurred at 70–50 Ma, coeval with that of the Dongjiangkou Granite in the eastern SQB, but later than the plutons in the western SQB, including the Liuba, Foping, and Ningshan granites, which is mainly induced by the faulting deformation. The Cuihuashan Granite in the eastern NQB started cooling with the sinistral deformation at around 60 Ma at the latest.

The third period of rapid cooling (50–20 Ma) at 2–5 °C/m.y. occurred mainly in the S-NCB and the eastern NQB, which was induced by the faulting and exhumation. At the same time the SQB and the western NQB were undergoing slow cooling at 0.15–0.6 °C/m.y. (Figs. 5–12), with the Mishuling Granite in the western SQB in particular being in a very stable state at this time (Fig. 8).

Moreover, most modeled *T–t* paths suggest a period of enhanced cooling since the late Cenozoic (~10 Ma; Figs. 5–12), similar to the apparently older (20 Ma) cooling phase in the Foping and Liuba Granites. However, this most recent period of rapid cooling involved below temperatures of 60 °C, which cannot be constrained using AFT data.

4. Integration of the results with previous data

In this paper, 45 samples were collected from eight Mesozoic granitoid plutons in the Qinling Orogen. The density and distribution of the samples cannot reveal the pattern of uplift and exhumation for the entire Qinling Orogen, especially given the absence of

Please cite this article in press as: Chen, H., et al. Apatite fission-track thermochronological constraints on the pattern of late Mesozoic–Cenozoic uplift and exhumation of the Qinling Orogen, central China. Journal of Asian Earth Sciences (2014), http://dx.doi.org/10.1016/j.jseaes.2014.10.004

samples from the N-SCB. Previous AFT data have covered the entire Qinling Orogen (Enkelmann et al., 2006; Grimmer et al., 2002; Hu et al., 2006a,b, 2012; Liu et al., 2013; Wang et al., 2011b; Yang et al., 2013). In those previous studies, the westernmost samples were collected from the Huicheng Basin in western Qinling Orogen (Wang et al., 2011b), the northernmost samples were taken from the Huashan Granite (Liu et al., 2013; Wan et al., 2000; Yin et al., 2001), the southernmost samples were obtained from the Sichuan Basin (Shen et al., 2007; Shi et al., 2012), and the easternmost samples were collected in the Dabie Terrane (Grimmer et al., 2002; Hu et al., 2006b). Furthermore, the uplift of the Hannan–Micangshan massif has been particularly well constrained (Hu et al., 2012; Tian et al., 2010; Yang et al., 2013). The samples of previous studies consisted of sedimentary, metamorphic, or granitic rocks of Proterozoic–Cenozoic age, but were dominated by Mesozoic granites. In this paper, we comprehensively analyzed 423 AFT ages (Fig. 2) and 145 modeling paths (Fig. 13) for the Qinling Orogen to reveal the spatial and temporal patterns of uplift and exhumation during the Mesozoic–Cenozoic (Chen et al., 1995; Enkelmann et al., 2006; Grimmer et al., 2002; Hu et al., 2006a,b, 2012; Li et al., 2010a; Liu et al., 2009, 2013; Shen et al., 2007; Tian et al., 2010; Wang and Yang, 1998; Wan et al., 2000, 2005; Wang et al., 2011b; Xu et al., 2005, 2010; Yang et al., 2013; Yin et al., 2001; Yu et al., 2013).

The results show that the timing of cooling clearly differed between the various micro-blocks (Fig. 13), being characterized by earlier cooling in the south of the orogen, consistent with transect studied in the east by Hu et al. (2006a). The S-NCB started to be cooled in the early Cenozoic, as shown by the uplift of the Lantian Granite (Enkelmann et al., 2006; Hu et al., 2006a), the Huashan Granite (Liu et al., 2013), and the Wenyu Granite (Yu et al., 2013). The NQB was cooling initially during the Late Cretaceous, and continued into the Cenozoic, as shown by the Baoji, Cuihuashan, and Taibai Granites (Figs. 6 and 7; Liu et al., 2013; Wan et al., 2005). The SQB, comprising the NW-SQB and the SE-SQB, started to be cooled at the end of the Early Cretaceous, as shown by the Mishuling, Liuba, Foping, and Ningshan Granites in the NW-SQB (Figs. 8–10; Enkelmann et al., 2006; Liu et al., 2013; Wang et al., 2011b) and by the Fenghuangshan Granite (Li et al., 2010a) and the Wudang dome (Hu et al., 2006a) in the SE-SQB. The prolongation of cooling differed between the NW-SQB and the SE-SQB with respect to Cenozoic cooling (Fig. 13). The Cenozoic cooling in the NW-SQB was characterized by the uplift of a Cenozoic basin in western Qinling Orogen (Wang et al., 2011b) and the eastern Dongjiangkou Granite (Fig. 12). The N-SCB cooling was prolonged, extending from the Late Jurassic to the early Cenozoic. The earliest cooling involved mainly the Hannan–Micangshan massif (Hu et al., 2012; Tian et al., 2010; Xu et al., 2010; Yang et al., 2013) and the Huangling Granite (Hu et al., 2006a, 2012), and the rapid cooling during the Cretaceous has also been revealed by data from the southern Dabashan belt (Shen et al., 2007; Shi et al., 2012) and from the northern Sichuan Basin (Yang et al., 2013). Both the N-SCB and the SE-SQB were stable or slow cooling during the Cenozoic. Our modeling results

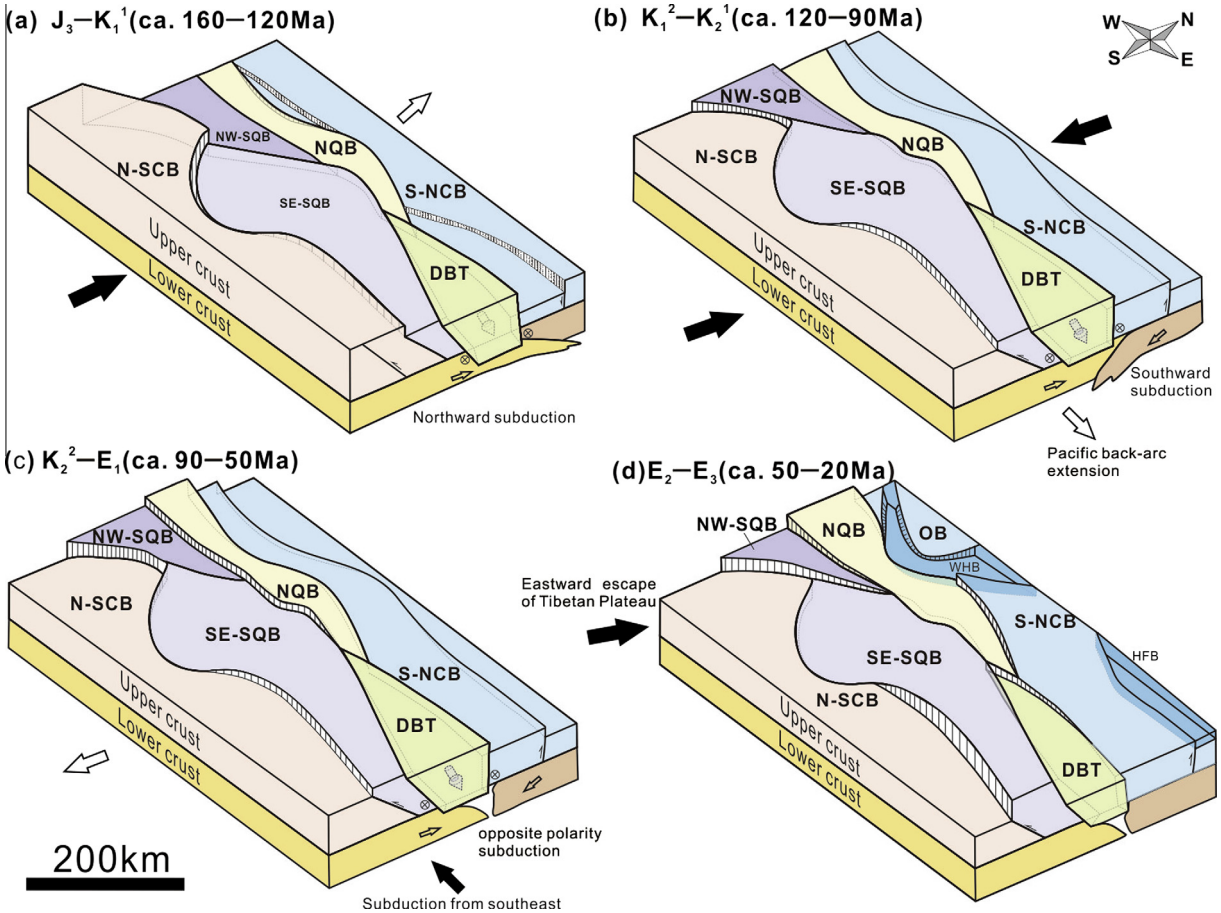

Fig. 14. Intracontinental cooling histories of the Qinling Orogen since the Late Jurassic. (a) During the Late Jurassic–Early Cretaceous (ca. 160–120 Ma), the initial cooling was limited to the N-SCB. (b) During the late Early Cretaceous–early Late Cretaceous (ca. 120–90 Ma), extensional and compressing related cooling was initiated in the SQB. (c) During the latest Cretaceous–Paleocene (ca. 90–50 Ma), regional-scale rapid uplift and exhumation was initiated in the NQB and subsequently extended over the entire Qinling Orogen apart from the S-NCB. (d) During the Eocene–Oligocene (ca. 50–20 Ma), faulting-related uplift and exhumation was initiated in the S-NCB and also continued in the NQB and NW-SQB.

Please cite this article in press as: Chen, H., et al. Apatite fission-track thermochronological constraints on the pattern of late Mesozoic–Cenozoic uplift and exhumation of the Qinling Orogen, central China. Journal of Asian Earth Sciences (2014), http://dx.doi.org/10.1016/j.jseaes.2014.10.004

suggest that the Qinling Orogen experienced an earlier stage of rapid cooling, during the Late Jurassic (Fig. 13), which differs from our new AFT data obtained from the Mesozoic granites. This difference may be related to the absence of samples from the N-SCB in the present study (Fig. 2).

5. Discussion

Previous research has proposed that the Qinling Orogen experienced regional uplift and exhumation during the Cretaceous (Hu et al., 2006a; Shen et al., 2007), which was coeval with the deposition of red layers in the Cretaceous continental-facies basin and the development of major strike-slip fault in the Qinling Orogen (Guo et al., 2009; Ratschbacher et al., 2003), although the N-SCB was cooling initially during the Eocene. Although the uplift and exhumation usually induced by the tectonics (Dumitru et al., 1991; Harrison et al., 1995, 1996, 2000; Spotila et al., 1998), magma intrusion and climate change (Li et al., 2014; Shuster et al., 2005), the AFT data can only revealed cooling history of the rock, which may be related to the uplift of the rock, surface uplift, exhumation and erosion (England and Molnar, 1990). Influenced by the Meso-Cenozoic intracontinental deformation, the granitic plutons were generally superposed by the faults with different character (e.g. thrust, normal and slip) (Fig. 3). The detailed tectonic analysis for granites will combine the cooling history with the tectonic effect.

Our new AFT data from Mesozoic granites and modeled *T*–*t* paths of previous data reveal a pattern of temporal and spatial variability in cooling history in the Qinling Orogen since the Cretaceous (Fig. 13; Enkelmann et al., 2006), rather than uniform regional rapid cooling across the entire Qinling Orogen. During the Cenozoic, the S-NCB, NQB, and NW-SQB underwent rapid cooling at the same time as the N-SCB and SE-SQB stabilized or cooled only slowly. This pattern of cooling history, and the northward younging of the cooling (Hu et al., 2006a), indicate that the uplift and exhumation of the Qinling Orogen was not uniform, but rather was specific for each constituent micro-block (Ratschbacher et al., 2003; Zhang et al., 2001).

The Qinling Orogen underwent intracontinental deformation during the Late Triassic (Zhang et al., 2001), and entered a period of convergence and collision during the Late Triassic–Middle Jurassic that propagated from east to west (Liu et al., 2005; Ratschbacher et al., 2003) and which ceased during the Middle Jurassic (Yang et al., 1992). During the collision, the largest known ultrahigh-pressure metamorphic Dabie Terrane was formed, rapid uplift and exhumation of the DBT subsequently occurred (Hacker et al., 2000; Li et al., 2010b; Tu et al., 2012). A series of Triassic–Jurassic granites was emplaced in extensional settings or in transitional settings (from compression to extension) in the western part of Qinling Orogen, particularly in the NW-SQB (Wang et al., 2011a; Zhang et al., 2008). During the early part of the intracontinental deformation stage that followed the Late Triassic, the Qinling Orogen underwent mainly block faulting, rifting, and strike-slip deformation. The deposition of continental-facies sediments and the formation of intermontane fault-bound basins, pull-apart basins, and foreland and hinterland basins also developed along both the northern and southern sides of the orogen (Zhang et al., 2001). During the Middle–Late Jurassic, the Qinling Orogen was characterized by intensive intracontinental subduction and thrust-nappe deformation (Dong et al., 2006; Zhang et al., 2001). Strike-slip movements and lateral extrusion along the orogen margins developed during the later collision period (Chen et al., 2010; Hu et al., 2011; Li et al., 2010b; Wang et al., 2003). The orogen entered the intracontinental orogenic stage during the Late Jurassic (Dong et al., 2006; Zhang et al., 2001).

Considering the timings of rapid cooling for the various micro-blocks, we are able to divide the late Mesozoic–Cenozoic intracontinental orogeny and cooling history of the Qinling Orogen into four stages, occurring during the Late Jurassic–Early Cretaceous (ca. 160–120 Ma), late Early Cretaceous–early Late Cretaceous (ca. 120–90 Ma), latest Cretaceous–Paleocene (ca. 90–50 Ma), and Eocene–Oligocene (ca. 50–20 Ma) (Fig. 13), as discussed in turn below.

5.1. Stage 1: Late Jurassic–Early Cretaceous cooling history

During the Late Jurassic–Early Cretaceous (ca. 160–120 Ma), the Qinling Orogen underwent postorogenic continental deformation and a stage of initial uplift (Fig. 14a). The AFT statistics and modeling results reveal that rapid cooling of the N-SCB began during the Late Jurassic at latest (Fig. 13; Hu et al., 2006a; Liu et al., 2009; Yang et al., 2013), as for the DBT to the east (Hu et al., 2006b; Meng et al., 2007; Wang and Yang, 1998). There is some variation in the pattern of cooling from east to west in the N-SCB, according to the age statistics and distribution (Fig. 2). Uplift was most pronounced in the Hannan–Micangshan massif and the Huangling Granite, which are separated by the Dabashan tectonic belt in the N-SCB, and the Huangling Granite was uplifted earlier than the Hannan–Micangshan massif during this stage (Xu et al., 2010). This temporal variation inn uplift may be related to the curved boundary of the N-SCB (Zhang et al., 2010), with the exhumation being related to deformation associated with the development of an intracontinental foreland (Xu et al., 2010; Yang et al., 2013).

The AFT data of the present study do not record any cooling in the micro-blocks to the north of the N-SCB (the S-NCB, NQB, and SQB) during this Late Jurassic–Early Cretaceous period. However, previous studies show that the Fenghuangshan Granite in the SE-SQB was uplifted later than the Hannan–Micangshan massif, as these two bodies were similar in the rock composition and time, and are separated by the Mianlue Suture (Li et al., 2010a; Yang et al., 2013). This difference in the timing of cooling between the two bodies is comparable with the differences in tectonic characteristics during this stage between the N-SCB on the one hand and the S-NCB, NQB, and SQB on the other.

With respect to tectonic deformation, the N-SCB during this stage was characterized by the development of thrust-nappe structures caused by intracontinental subduction (Dong et al., 2006; Hu et al., 2012; Li et al., 2010b; Shi et al., 2012), together with a series of foreland basins (Liu et al., 2005), whereas deformation in the S-NCB, SQB, and DBT was characterized mainly by extensional and strike-slip tectonics (Cui et al., 2012; Hu et al., 2011; Li et al., 2010b; Lin et al., 2005; Ratschbacher et al., 2000) and a series of extensional basins (Meng et al., 2007). During this stage, the S-NCB and NQB were the sites of magmatic activity (Dong et al., 2011a) that was closely related to lithospheric thinning and asthenosphere upwelling of the NCB during the early Cretaceous, and as yet there is no similar Cretaceous magmatism reported in the N-SCB. During this first stage, the sedimentary center of the continental foreland basin in the N-SCB shifted to the northern Sichuan Basin, and uplift began in the Zigui Basin, related to southward thrusting (Liu et al., 2005). The Hefei Basin, an extensional faulted basin in the S-NCB, began to be uplifted during the Early Cretaceous (Meng et al., 2007).

Therefore, the Qinling Orogen was characterized by uplift in the south and subsidence in the north during the Late Jurassic–Early Cretaceous. Meanwhile, the South China Block subducted northwards toward the Qinling Orogen and rotated clockwise (Meng et al., 2005; Ratschbacher et al., 2003), a process that was influenced by the opening of the Neo-Tethys, the northward accretion of the Cimmerian continent, and the westward subduction of the Pacific Plate (Ratschbacher et al., 2003; Sengor, 1992). At the same

Please cite this article in press as: Chen, H., et al. Apatite fission-track thermochronological constraints on the pattern of late Mesozoic–Cenozoic uplift and exhumation of the Qinling Orogen, central China. Journal of Asian Earth Sciences (2014), http://dx.doi.org/10.1016/j.jseaes.2014.10.004

time, the S-NCB was located at the trailing edge of the extensional environment, which was formed by multi-directional convergent motion, including the northward subduction of the South China Block and the westward subduction of the Pacific Plate (Dong et al., 2008; Meng et al., 2007). Therefore, the exhumation of the Qinling Orogen was associated with the clockwise rotation of the South China Block and its northward subduction (Hu et al., 2006a; Ratschbacher et al., 2003; Yang et al., 2013; Zhang et al., 2001).

5.2. Stage 2: late Early Cretaceous–early Late Cretaceous cooling history

During the late Early Cretaceous–early Late Cretaceous (ca. 120–90 Ma), the Qinling orogen was affected by NE–SW compressional and NW–SE extensional stress fields associated with the eastward tectonic escape resulting from the Lhasa–Qiangtang Indochina collision and Pacific back-arc extension (Fig. 14b; Dong et al., 2011a; Hu et al., 2006a; Ratschbacher et al., 2003; Zhang et al., 2001). The AFT data reveal that rapid cooling were initiated in the SQB and also continued in the N-SCB (Fig. 13). The N-SCB is characterized by the development of the southern Dabashan belt (Shen et al., 2007; Xu et al., 2010). In the SQB, this earliest stage of cooling involved the western NW-SQB (e.g., the Mishuling and Liuba Granites) and the western SE-SQB (e.g., the Fenghuangshan Granite), whereas the eastern NW-SQB and SE-SQB were cooling later, including the Foping and Ningshan granites (at ~110 Ma) and the Wudang dome (after 100 Ma) (Hu et al., 2006a). The eastward younging of cooling is identical to the pattern established during the whole of the Cretaceous–Cenozoic (Enkelmann et al., 2006).

The western parts of both the SQB and NQB, and the southern Dabashan belt underwent rapid cooling during the Early Cretaceous (Shen et al., 2007; Li et al., 2010a; Wang et al., 2011b). Also at this time, the Qiangtang and Lhasa blocks collided to the southwest of the Qinling Orogen, and the South China Block continued its northward intracontinental subduction (Ratschbacher et al., 2003). During the Early Cretaceous, the simultaneous westward subduction of the Pacific Plate and the southward-directed pressure of the Siberia Plate caused the North China Block to subduct southwards (Ratschbacher et al., 2003). During the North China Block intracontinental subduction under the Qinling Orogen, the strong southward-directed thrust-nappe structures were formed in the NQB and west of SQB (Fig. 3; Zhang et al., 2001), causing limited but rapid cooling and uplift of the Baoji Granite in the NQB, and Mishuling and Liuba Granites in the SQB (Fig. 6). Thus, we suggest that this rapid uplift occurred in response to southward subduction of the North China Block and to the broadly extensional deformation in the eastern China continent, both of which were associated with convergence of the Siberia Plate, the Pacific Plate, and the Qiangtang Block during the Early Cretaceous (Dong et al., 2008; Ratschbacher et al., 2003).

Consistent with the rapid cooling in the NQB and SQB in this tectonic regime, rifting in the Qinling Orogen occurred at early Cretaceous (Hu et al., 2006a; Ratschbacher et al., 2003). A series of Cretaceous basins (e.g., the Huicheng and Shiyan basins) and extensional domes (e.g., the Foping and Wudang domes) developed, distributed mainly in the western NW-SQB and the eastern SE-SQB and N-SCB (Fig. 2). The extensional domes mainly located at the middle SQB, and induced the rapid cooling and uplift at cooling rate 1.5–2.5 °C/m.y. in the Foping and Ningshan Granites. These basins extended along ENE–WSW- and NW–SE-trending conjugate faults, also reflecting the E–W-directed extensional stress field (Ratschbacher et al., 2003). Particular to the DBT, rapid uplift was most noticeable during this stage (Chen et al., 1995), and the uplift resulted from the continuing tectonic extrusion of the DBT from the Jurassic onwards (Tu et al., 2012; Wang et al., 2003).

5.3. Stage 3: latest Cretaceous–Paleocene cooling history

In the Late Cretaceous, the Qinling Orogen entered a new stage of rapid uplift and exhumation during the latest Cretaceous–Paleocene (ca. 90–50 Ma), which was related to a reversal in the direction of maximum compressive stress field between the Early and Late Cretaceous (Fig. 14c; Ratschbacher et al., 2003). Except the S-NCB, the entire Qinling Orogen experienced this period of rapid cooling initially occurring in the NQB (Fig. 13; Hu et al., 2006a). The N-SCB was characterized by rapid cooling in the southern Dabashan belt (Shen et al., 2007) and in the Huangling Granite (Hu et al., 2006a), and by slow uplift and exhumation in the Hannan–Micangshan massif (Yang et al., 2013). Cooling of the SQB propagated both to the east (e.g., the Dongjiangkou Granite and Wudang dome) and to the west in the NW-SQB (e.g., the Mishuling, Liuba, and Foping granites), and was superimposed over the ongoing period of rapid cooling. This superimposition also led to the Mesozoic granites, including the Foping, Liuba, and Ningshan granites, being uplifted to higher elevations than were attained during the second stage of uplift (late Early Cretaceous–early Late Cretaceous) (Fig. 3).

This third stage was characterized by widespread exhumation of the Qinling Orogen (Enkelmann et al., 2006; Grimmer et al., 2002; Hu et al., 2006a; Li et al., 2010a; Wang et al., 2011b; Xu et al., 2010; Yang et al., 2013), corresponding to the regional uplift and exhumation identified in previous studies (Hu et al., 2006a; Shen et al., 2007). Simultaneously, widespread Late Cretaceous–Tertiary extensional basins developed in the northern Qinling Orogen (Fig. 2; Ratschbacher et al., 2003; Zhang et al., 2001). These basins were distributed not only along early E–W-trending faults (e.g., the Shangluo Basin), but also along conjugate shear fractures with NW–SE- and NE–SW-trending faults (e.g., the Huixian–Chengxian and Luoyang basins) (Fig. 2), recording a NE–SW extensional stress field from the Late Cretaceous to the Paleocene (Enkelmann et al., 2006; Ratschbacher et al., 2003). Through the early Late Cretaceous, the geodynamic regime changed in southeastern Asia because of the subduction of the Izanagi Plate to the southeast, and the stress field changed to overall NW–SE compression and NE–SW extension with sinistral slip on N–S- or NE–SW-trending faults and dextral slip along ESE–WNW-trending fault zones (Ratschbacher et al., 2003), such as the sinistral fault in the Ningshan Granite, and induced the uplift of the granite. Meanwhile, the northern and southern boundaries of the Qinling Orogen underwent intracontinental subduction with opposite polarity during the Late Cretaceous (Dong et al., 2011a; Ratschbacher et al., 2003; Zhang et al., 2003), such as the sustained thrust in the Baoji Granite. Therefore, we consider that the rapid uplift and exhumation during the Latest Cretaceous–Paleocene was caused by the change in the stress field and the opposite polarity subduction.

5.4. Stage 4: Eocene–Oligocene cooling history

During the Eocene–Oligocene (ca. 50–20 Ma), a period of basin faulting affected the Qinling Orogen, characterized by the exhumation initiated in the S-NCB (Fig. 14d). Several fission-track studies, structural and sedimentological investigations, and climatic change studies have proposed that the northern margin of the Qinling Orogen was characterized by multiple stages of rapid uplift and exhumation during the Cenozoic (Kaakinen and Lunkka, 2003; Mercier et al., 2013; Li et al., 2014; Liu et al., 2013; Zhang et al., 1995, 1998, 2003). Our new data show that the S-NCB started to be cooled during the Eocene, as did the NQB and NW-SQB (Fig. 13), especially in the southern region of the Weihe Basin, and including the Hua Shan and Taibai Shan uplifts (Heberer et al., 2014; Hu et al., 2006a; Liu et al., 2013).

Please cite this article in press as: Chen, H., et al. Apatite fission-track thermochronological constraints on the pattern of late Mesozoic–Cenozoic uplift and exhumation of the Qinling Orogen, central China. Journal of Asian Earth Sciences (2014), http://dx.doi.org/10.1016/j.jseaes.2014.10.004

Also at this time, the Weihe Basin between the Qinling Orogen and the Ordos Block began to undergo rifting (Zhang et al., 1998), which suggests that the formation of the Weihe Basin was closely related to the uplift and normal fault of the northern margin of the Qinling Orogen (Liu et al., 2013; Zhang et al., 2001), such as the Lantian and Baoji Granites. The Weihe Basin experienced extensive Cenozoic rifting, and the height difference between the Cenozoic strata at the bottom of the Weihe Basin and the top of the Taibai Shan (elevation 3767 m) is approximately 10 km (Zhang et al., 2001); this rifting uplift forms a boundary separating the North China and South China blocks geologically, biologically, and climatologically (Ge et al., 2013; Han et al., 2001; Liu et al., 2013; Zhang et al., 2001).

During the early Cenozoic, the NW-SQB also underwent rapid cooling, recorded by the exhumation and uplift of Tertiary basins (Wang et al., 2011b) and Mesozoic granites (e.g., the Liuba, Ningshan, and Dongjiangkou granites). In contrast, the SQB and N-SCB underwent slow cooling at <1 °C/m.y. during the early Cenozoic (Fig. 13; Yang et al., 2013). Therefore, the driving force for the rapid cooling at north may have originated from the southwest. In addition, the formation of the Weihe Basin and uplift in the S-NCB and NW-SQB occurred simultaneously with continental collision between the Indian and Eurasian plates (Liao et al., 2007; Yin and Harrison, 2000), indicating that the tectonic uplift was related to northeastward-directed compressive stress resulting from the eastward tectonic escape of Tibetan Plateau imposed by India–Asia collision starting at ~50 Ma (Enkelmann et al., 2006; Liu et al., 2004; Ratschbacher et al., 2003; Yin and Harrison, 2000). Although the climate change maybe another important effect for the surface exhumation and erosion (Shuster et al., 2005), the climate change in Qinling Orogen and northeast Tibetan Plateau was also related to the uplift of the Tibetan Plateau and India–Asia continental collision in early Cenozoic (Li et al., 2014).

Since the late Miocene (~10 Ma), the latest stage of cooling has affected the northeastern margin of the Tibetan Plateau (Enkelmann et al., 2006; Ge, 2012; Hu et al., 2006a; Liu et al., 2013; Wang et al., 2011b; Zhang et al., 1991), and has been most noticeable in the Longmen Shan tectonic belt (Li et al., 2012; Meng et al., 2006; Wang et al., 2012). This rapid cooling has occurred in association with the northeastern extension of the Tibetan Plateau, as shown by AFT data (Enkelmann et al., 2006; Yang et al., 2013); however, the AFT modeling data provide only minimal control on the timing of the uplift, similar to the control placed by our data on the most recent stage of rapid cooling in the present study area (Figs. 5–12). Thus, we consider that rapid late-Cenozoic uplift and exhumation occurred in the Qinling Orogen and formed the current noticeable step-like topography of the Chinese mainland (Fig. 1).

It is generally understood that the Qinling Orogen was not formed by collisional orogenesis in the main orogenic period during the Triassic–Middle Jurassic, but rather by uplift and exhumation during a period of intracontinental orogeny since the Late Jurassic (Zhang et al., 2001). Uplift and exhumation of the Qinling Orogen was characterized by the propagation of rapid cooling from south to north, and the cooling histories of the micro-blocks are consistent with the pattern of intracontinental deformation and with their separation by the main tectonic boundaries such as the Mianlue Suture and the Ningshan Fault.

6. Conclusions

The apatite fission-track ages and thermal modeling of 45 Mesozoic granitic samples from eight plutons in three micro-blocks show that the Qinling Orogen experienced four stages of cooling histories during the late Mesozoic and Cenozoic: (1) initial cooling during the Late Jurassic–Early Cretaceous (ca. 160–120 Ma) was limited to the N-SCB; (2) initiated rapid cooling in the SQB during the late Early Cretaceous–early Late Cretaceous (ca. 120–90 Ma) induced by the compression and extensional deformation; (3) regional-scale rapid cooling during the latest Cretaceous–Paleocene (ca. 90–50 Ma) was initiated in the NQB and subsequently extended throughout the Qinling Orogen apart from the S-NCB; and (4) Tibetan Plateau expanding- and fault-related cooling initiated in the S-NCB during the Eocene–Oligocene (ca. 50–20 Ma) and continued in the NQB and NW-SQB.

Uplift and exhumation in the Qinling Orogen propagated from south to north during the late Mesozoic–Cenozoic, consistent with the record of intracontinental deformation, magmatism, and development of sedimentary basins.

The various micro-blocks of the Qinling Orogen were uplifted and exhumed at different times and rates, which suggests that the intracontinental deformation was controlled by existing collisional belts and tectonic boundaries.

Acknowledgements

We thank Prof. Jolivet M. and Prof. Yin A. for reviewing an earlier draft of this paper and for providing constructive suggestions. We are also very grateful to anonymous reviewers for their constructive and thorough reviews of the manuscript. This work was funded by the National Science Foundation of China (41102126 and 91114204) and the Chinese Government's Executive Program (SinoProbe-08-01-03), and China Geological Survey Program (1212011220259).

References

Chen, J., Xie, Z., Liu, S., Li, X., Foland, K.A., 1995. The cooling age of 40Ar–39Ar and fission track dating in Dabie Orogenic belt. Sci. China Chim. 25 (10), 1086–1092 (in Chinese).

Chen, H., Hu, J., Wu, G., Gao, W., 2010. Study on the intracontinental deformation of the Mian-Lue suture belt, western Qinling. Acta Petrol. Sin. 26 (4), 1277–1288 (in Chinese with English abstract).

Cui, J., Liu, X., Dong, S., Hu, J., 2012. U–Pb and 40Ar/39Ar geochronology of the Tongbai complex, central China: implications for Cretaceous exhumation and lateral extrusion of the Tongbai-Dabie HP/UHP terrane. J. Asian Earth Sci. 47, 155–170.

Donelick, R.A., Ketcham, R.A., Carlson, W.D., 1999. Variability of apatite fission-track annealing kinetics II: Crystallographic orientation effects. Am. Mineral. 84, 1224–1234.

Donelick, R.A., Sullivan, P.B.O., Ketcham, R.A., 2005. Apatite fission-track analysis. Rev. Mineral. Geochem. 58, 49–94.

Dong, Y., Zhang, G., Lai, S., Zhou, D., Zhu, B., 1999. An ophiolitic tectonic melange first discovered in Huashan area, south margin of Qinling Orogenic Belt, and its tectonic implications. Sci. China Earth Sci. 42 (3), 292–302.

Dong, S., Hu, J.M., Shi, W., Zhang, Z., Liu, G., 2006. Jurassic superposed folding and Jurassic foreland in the Daba mountain, central China. Acta Geosci. Sin. 27 (5), 403–410 (in Chinese with English abstract).

Dong, S., Zhang, Y., Long, C., Yang, Z., Ji, Q., Wang, T., Hu, J., Chen, X., 2008. Jurassic Tectonic revolution in China and new interpretation of the "Yanshan Movement". Acta Geol. Sin. 82 (2), 334–347.

Dong, Y., Zhang, G., Neubauer, F., Liu, X., Genser, J., Hauzenberger, C., 2011a. Tectonic evolution of the Qinling orogen, China: review and synthesis. J. Asian Earth Sci. 41 (3), 213–237.

Dong, Y., Zhang, G., Hauzenberger, C., Neubauer, F., Yang, Z., Liu, X., 2011b. Palaeozoic tectonics and evolutionary history of the Qinling orogen: evidence from geochemistry and geochronology of ophiolite and related volcanic rocks. Lithos 122 (1–2), 39–56.

Dong, Y., Liu, X., Zhang, G., Chen, Q., Zhang, X., Li, W., Yang, C., 2012. Triassic diorites and granitoids in the Foping area: constraints on the conversion from subduction to collision in the Qinling orogen, China. J. Asian Earth Sci. 47, 123–142.

Dumitru, T.A., Gans, P.B., Foster, D.A., Miller, E.L., 1991. Refrigeration of the western Cordilleran lithosphere during Laramide shallow-angle subduction. Geology 19 (11), 1145–1148.

England, P., Molnar, P., 1990. Surface uplift, uplift of rocks, and exhumation of rocks. Geology 18 (12), 1173–1177.

Enkelmann, E., Ratschbacher, L., Jonckheere, R., Nestler, R., Fleischer, M., Gloaguen, R., Hacker, B.R., Zhang, Y.Q., Ma, Y., 2006. Cenozoic exhumation and deformation of northeastern Tibet and the Qinling: is Tibetan lower crustal flow diverging around the Sichuan Basin? Geol. Soc. Am. Bull. 118 (5–6), 651–671.

Galbraith, R.F., 1981. On statistical models for fission track counts. J Int. Ass. Math. Geol. 13 (6), 471–478.
Galbraith, R.F., Laslett, G.M., 1993. Statistical models for mixed fission track ages. Nucl. Tracks 21, 459–470.
Ge, J., 2012. Magnetostratigraphy of the Xihe loess-soil sequence and implication for late Neogene uplift of the West Qinling Mountains. Quatern. Int. 163, 279–280.
Ge, J., Dai, Y., Zhang, Z., Zhao, D., Li, Q., Zhang, Y., Yi, L., Wu, H., Oldfield, F., Guo, Z., 2013. Major changes in East Asian climate in the mid-Pliocene: triggered by the uplift of the Tibetan Plateau or global cooling? J. Asian Earth Sci. 69, 48–59.
Gleadow, A.J.W., Duddy, I.R., Green, P.F., 1986. Confined fission track lengths in apatite: a diagnostic tool for thermal history analysis. Contrib. Mineral. Petrol. 94, 405–415.
Gleadow, A., Belton, D., Kohn, B., Brown, R., 2002. Fission track dating of phosphate minerals and the thermochronology of apatite. Rev. Mineral. Geochem. 48, 579–630.
Green, P.F., 1981. Anew look at statistics in fission track dating. Nucl. Tracks 9 (5), 77–86.
Green, P.F., 1986. On the thermo-tectonic evolution of northern England: evidence from fission track analysis. Geology 5, 493–506.
Grimmer, J.C., Jonckheere, R., Enkelmann, E., Ratschbacher, L., Hacker, B.R., Blythe, A.E., Wagner, G.A., Wu, Q., Liu, S., Dong, S., 2002. Cretaceous–Cenozoic history of the southern Tan-Lu fault zone: apatite fission-track and structural constraints from the Dabie Shan (eastern China). Tectonophysics 359 (3–4), 225–253.
Guo, J., Han, W., Li, X., 2009. The Cenozoic Tectonic evolution of the West Qinling: constraints on the uplift and deformation of the Qinghai-Tibet Plateau. Earth Sci. Front. 16 (6), 215–225.
Hacker, B.R., Ratschbacher, L., Webb, L.E., McWilliams, M., Ireland, T., Calvert, A., Dong, S., Wenk, H., Chateigner, D., 2000. Exhumation of ultrahigh-pressure continental crust in east central China: Late Triassic–Early Jurassic tectonic unroofling. J. Geophys. Res. 105 (86), 13339–13364.
Han, H., Mi, F., Liu, H., 2001. Geomorphological structure in the Weihe Basin and Neotectonic movement. J. Seismol. Res. 24 (3), 251–257 (in Chinese with English abstract).
Harrison, T.M., Copeland, P., Kidd, W.S.F., Lovera, O.M., 1995. Activation of the Nyainqentanghla shear zone: implications for uplift of the southern Tibetan Plateau. Tectonics 14 (3), 658–676.
Harrison, T.M., Leloup, P.H., Ryerson, F.J., Tapponnier, P., Lacassin, R., Chen, W., 1996. Diachronous initiation of transtension along the Ailao Shan-Red River shear zone, Yunnan and Vietnam. In: Yin, A., Harrison, T.M. (Eds.), The Tectonic Evolution of Asia. Cambridge University Press, Cambridge, UK, pp. 208–226.
Harrison, T.M., Yin, A., Grove, M., Lovera, O.M., Ryerson, F.J., Zhou, X., 2000. The Zedong window: a record of superposed Tertiary convergence in southeastern Tibet. J. Geophys. Res.: Solid Earth 105 (B8), 19211–19230.
Heberer, B., Anzenbacher, T., Neubauer, F., Genser, J., Dong, Y., Dunkl, I., 2014. Polyphase exhumation in the western Qinling Mountains, China: rapid Early Cretaceous cooling along a lithospheric-scale tear fault and pulsed Cenozoic uplift. Tectonophysics 617, 31–43.
Hu, S., Raza, A., Kohn, B.P., Reiners, P.W., Ketcham, R.A., Wang, J., Gleadow, A.J.W., 2006a. Late Mesozoic and Cenozoic thermotectonic evolution along a transect from the north China craton through the Qinling orogen into the Yangtze craton, central China. Tectonics 25 (6), 1029–1044.
Hu, S., Kohn, B.P., Raza, A., Wang, J., Gleadow, A.J.W., 2006b. Cretaceous and Cenozoic cooling history across the ultrahigh pressure Tongbai-Dabie belt, central China, from apatite fission-track thermochronology. Tectonophysics 420 (3–4), 409–429.
Hu, J., Meng, Q., Chen, H., Wu, G., Qu, H., Gao, W., Chen, W., 2011. Tectonic evolution and implication of Ningshan Fault in the central part of Qinling Orogen. Acta Petrol. Sin. 27 (3), 657–671 (in Chinese with English abstract).
Hu, J., Chen, H., Qu, H., Wu, G., Yang, J., Zhang, Z., 2012. Mesozoic deformations of the Dabashan in the southern Qinling orogen, central China. J. Asian Earth Sci. 47, 171–184.
Hurford, A.J., Green, P.F., 1982. A users' guide to fission-track dating calibration. Earth Planet Sci. Lett. 59, 343–354.
Jiang, Y., Jin, G., Liao, S., Zhou, Q., Zhao, P., 2010. Geochemical and Sr–Nd–Hf isotopic constraints on the origin of Late Triassic granitoids from the Qinling orogen, central China: implications for a continental arc to continent–continent collision. Lithos 117 (1–4), 183–197.
Kaakinen, A., Lunkka, J.P., 2003. Sedimentation of the Late Miocene Bahe Formation and its implications for stable environments adjacent to Qinling mountains in Shaanxi, China. J. Asian Earth Sci. 22 (1), 67–78.
Ketcham, R.A., 2005. Forward and inverse modeling of low-temperature thermochronometry data. Rev. Mineral. Geochem. 58, 275–314.
Ketcham, R.A., 2009. HeFTy Version 1.6.7. The University of Texas, Austin, pp. 1–65.
Ketcham, R.A., Donelick, R.A., Carlson, W.D., 1999. Variability of apatite fission-track annealing kinetics III: Extrapolation to geological time scales. Am. Mineral. 84, 1235–1255.
Ketcham, R.A., Carter, A., Donelick, R.A., Barbarand, J., Hurford, A.J., 2007. Improved modeling of fission-track annealing in apatite. Am. Mineral. 92, 799–810.
Lai, S., Zhang, G., Dong, Y., Pei, X., Chen, L., 2004. Geochemistry and regional distribution of ophiolites and associated volcanics in Mianlue suture, Qinling-Dabie Mountains. Sci. China Earth Sci. 47 (4), 289–299.
Li, S., Kusky, T.M., Wang, L., Zhang, G., Lai, S., Liu, X., Dong, S., Zhao, G., 2007. Collision leading to multiple-stage large-scale extrusion in the Qinling orogen: insights from the Mianlue suture. Gondwana Res. 12 (1–2), 121–143.
Li, J., Zhang, Y., Dong, S., Shi, W., Li, H., 2010a. Apatite fission track therm ochronologic constraint on Late Mesozoic uplifting of the Fenghuangshan basement uplift. Chin. J. Geol. 45 (4), 969–986 (in Chinese with English abstract).
Li, S., Kusky, T.M., Zhao, G., Liu, X., Zhang, G., Kopp, H., Wang, L., 2010b. Two-stage Triassic exhumation of HP-UHP terranes in the western Dabie orogen of China: constraints from structural geology. Tectonophysics 490 (3–4), 267–293.
Li, Z., Liu, S., Chen, H., Deng, B., Hou, M., Wu, W., Cao, J., 2012. Spatial variation in Meso-Cenozoic exhumation history of the Longmen Shan thrust belt (eastern Tibetan Plateau) and the adjacent western Sichuan basin: constraints from fission track thermochronology. J. Asian Earth Sci. 47, 185–203.
Li, J., Fang, X., Song, C., Pan, B., Ma, Y., Yan, M., 2014. Late Miocene-Quaternary rapid stepwise uplift of the NE Tibetan Plateau and its effects on climatic and environmental changes. Quatern. Res. 81, 400–423.
Liao, Z., Mo, X., Pan, G., Zhu, D., Wang, L., Jiang, X., Zhao, Z., 2007. Spatial and temporal distribution of peraluminous granites in Tibet and their tectonic significance. J. Asian Earth Sci. 29 (2–3), 378–389.
Lin, W., Faure, M., Wang, Q.C., Arnaud, N., 2005. Tectonic evolution of Dabie Orogeny, in the view from polyphase deformation of Beihuaiyang metamorphic zone. Sci. China Earth Sci. 48 (7), 886–899.
Liu, M., Cui, X., Liu, F., 2004. Cenozoic rifting and volcanism in eastern China: a mantle dynamic link to the Indo-Asian collision? Tectonophysics 393 (1–4), 29–42.
Liu, S., Steel, R., Zhang, G., 2005. Mesozoic sedimentary basin development and tectonic implication, northern Yangtze Block, eastern China: record of continent–continent collision. J. Asian Earth Sci. 25 (1), 9–27.
Liu, H., Xu, C., Zhou, Z., Donelick, R.A., 2009. The formation of the Huangling uplift (165–100 Ma): constraints from the detrital apatite fission track thermochronology. Prog. Natl. Sci. 19 (12), 1326–1332 (in Chinese).
Liu, J., Zhang, P., Lease, R.O., Zheng, D., Wan, J., Wang, W., Zhang, H., 2013. Eocene onset and late Miocene acceleration of Cenozoic intracontinental extension in the North Qinling range-Weihe graben: insights from apatite fission track thermochronology. Tectonophysics 584, 281–296.
Lu, X., Wei, X., Xiao, Q., 1999. Geochronological studies of rapakivi granites in Qinling and its geological implications. Geol. J. China Univ. 5 (4), 372–377 (in Chinese with English abstract).
Mao, J., Xie, G., Zhang, Z., Li, X., Wang, Y., Zhang, C., Li, Y., 2005. Mesozoie large-scale metallogenic pulses in North China and corresponding geodynamic settings. Acta Petrol. Sin. 21 (1), 169–188 (in Chinese with English abstract).
Meng, Q.R., Zhang, G.W., 1999. Timing of collision of the North and South China blocks: controversy and reconciliation. Geology 27 (2), 123–126.
Meng, Q.R., Zhang, G.W., 2000. Geologic framework and tectonic evolution of the Qinling Orogen, central China. Tectonophysics 323 (3–4), 183–196.
Meng, Q., Wang, E., Hu, J., 2005. Mesozoic sedimentary evolution of the northwest Sichuan basin: implication for continued clockwise rotation of the South China block. Geol. Soc. Am. Bull. 117 (3–4), 396–410.
Meng, Q., Hu, J., Wang, E., Qu, H., 2006. Late Cenozoic denudation by large-magnitude landslides in the eastern edge of Tibetan Plateau. Earth Planet. Sci. Lett. 243 (1–2), 252–267.
Meng, Q., Li, S., Li, R., 2007. Mesozoic evolution of the Hefei basin in eastern China: sedimentary response to deformations in the adjacent Dabieshan and along the Tanlu fault. Geol. Soc. Am. Bull. 119 (7/8), 897–916.
Mercier, J.L., Vergely, P., Zhang, Y.Q., Hou, M.J., Bellier, O., Wang, Y.M., 2013. Structural records of the Late Cretaceous–Cenozoic extension in Eastern China and the kinematics of the Southern Tan-Lu and Qinling Fault Zone (Anhui and Shaanxi provinces, PR China). Tectonophysics 582 (2), 50–75.
Qin, J., Lai, S., Li, Y., 2008. Slab breakoff model for the triassic post-collisional adakitic granitoids in the Qinling Orogen, Central China: zircon U–Pb Ages, geochemistry, and Sr–Nd–Pb isotopic constraints. Int. Geol. Rev. 50, 1080–1104.
Qin, J., Lai, S., Grapes, R., Diwu, C., Ju, Y., Li, Y., 2009. Geochemical evidence for origin of magma mixing for the Triassic monzonitic granite and its enclaves at Mishuling in the Qinling orogen (central China). Lithos 112 (3–4), 259–276.
Ratschbacher, L., Hacker, B.R., Webb, L.E., McWilliams, M., Ireland, T., Dong, S., Calvert, A., Chateigner, D., Wenk, H., 2000. Exhumation of the ultrahigh-pressure continental crust in east central China: Cretaceous and Cenozoic unroofing and the Tan-Lu fault. J. Geophys. Res. 105 (B6), 13303–13338.
Ratschbacher, L., Hacker, B.R., Calvert, A., Webb, L.E., Grimmer, J.C., McWilliams, M.O., Ireland, T., Dong, S., Hu, J., 2003. Tectonics of the Qinling (Central China): tectonostratigraphy, geochronology, and deformation history. Tectonophysics 366 (1–2), 1–53.
Sengor, A.M.C., 1992. The palaeothethys suture a line of demarcation between two fundamentally different architectural style in the structure of Asia. Island Arc 1 (1), 78–91.
Shen, C., Mei, L., Xu, Z., Tang, J., Tian, P., 2007. Fission track thermochronology evidence for Mesozoic–Cenozoic uplifting of Daba Mountain, central China. Acta Petrol. Sin. 23 (11), 2901–2910 (in Chinese with English abstract).
Shi, W., Zhang, Y., Dong, S., Hu, J., Wiesinger, M., Ratschbacher, L., Jonckheere, R., Li, J., Tian, M., Chen, H., Wu, G., Ma, L., Li, H., 2012. Intra-continental Dabashan orocline, southwestern Qinling, Central China. J. Asian Earth Sci. 46, 20–38.
Shi, W., Li, J., Tian, M., Wu, G., 2013. The tectonic evolution of the Dabashan orocline, Central China: insights from superposed folds in the eastern Dabashan foreland. Geosci. Front. 4, 729–741.
Shuster, D.L., Ehlers, T.A., Rusmoren, M.E., Farley, K.A., 2005. Rapid glacial erosion at 1.8 Ma revealed by 4He/3He thermochronometry. Science 310, 1668–1670.
Spotila, J.A., Farley, K.A., Sieh, K., 1998. Uplift and erosion of the San Bernardino Mountains associated with transpression along the San Andreas fault,

Please cite this article in press as: Chen, H., et al. Apatite fission-track thermochronological constraints on the pattern of late Mesozoic–Cenozoic uplift and exhumation of the Qinling Orogen, central China. Journal of Asian Earth Sciences (2014), http://dx.doi.org/10.1016/j.jseaes.2014.10.004

California, as constrained by radiogenic helium thermochronometry. Tectonics 17 (3), 360–378.
Tagami, T., Sullivan, P.B.O., 2005. Fundamentals of fission-track thermochronology. Rev. Mineral. Geochem. 58, 19–47.
Tian, Y., Zhu, C., Xu, M., Rao, S., Barry, P.K., Hu, S., 2010. Exhumation history of the Micangshan-Hannan Dome since Cretaceous and its tectonic significance: evidences from Apatite Fission Track analysis. Chin. J. Geophys. 53 (4), 920–930 (in Chinese with English abstract).
Tu, X.B., Dai, F.C., Pan, Y.S., 2012. Dating of faults and estimation of surface uplift and erosion rates in the northern margin of Dabie Mountains, China. J. Asian Earth Sci. 56, 72–76.
Wan, J., Li, Q., Wang, Y., 2000. The fission track evidence of Huashan batholith uplifting in Mesozoic–Cenozoic. Seismol. Geol. 22 (1), 53–58 (in Chinese with English abstract).
Wan, J., Wang, Y., Li, Q., Zheng, D., Li, D., 2005. Apatite fission track study of Taibai Mountain uplift in the Mesozoic–Cenozoic. Nucl. Tech. 28 (9), 712–716 (in Chinese with English abstract).
Wang, G., Yang, W., 1998. Accelerated exhumation during the Cenozoic in the Dabie Mountains: evidence from fission-track ages. Acta Geol. Sin. 72 (4), 409–419.
Wang, E.C., Meng, Q.R., Burchfiel, B.C., Zhang, G.W., 2003. Mesozoic large-scale lateral extrusion, rotation, and uplift of the Tongbai-Dabie Shan belt in east China. Geology 31, 307–310.
Wang, X., Wang, T., Castro, A., Pedreira, R., Lu, X., Xiao, Q., 2011a. Triassic granitoids of the Qinling orogen, central China: genetic relationship of enclaves and rapakivi-textured rocks. Lithos 126 (3–4), 369–387.
Wang, X., Zattin, M., Li, J., Song, C., Peng, T., Liu, S., Liu, B., 2011b. Eocene to Pliocene exhumation history of the Tianshui-Huicheng region determined by apatite fission track thermochronology: implications for evolution of the northeastern Tibetan Plateau margin. J. Asian Earth Sci. 42 (1–2), 97–110.
Wang, E., Kirby, E., Furlong, K.P., van Soest, M., Xu, G., Shi, X., Kamp, P.J.J., Hodges, K.V., 2012. Two-phase growth of high topography in eastern Tibet during the Cenozoic. Nat. Geosci. 5, 640–645.
Wang, X., Wang, T., Zhang, C., 2013. Neoproterozoic, Paleozoic, and Mesozoic granitoid magmatism in the Qinling Orogen, China: constraints on orogenic process. J. Asian Earth Sci. 72, 129–151.
Xu, C., Zhou, Z., Haute, P.V.D., Donelick, R.A., Grave, J.D., Ma, C., Reiners, P.W., 2005. Apatite-fission-track geochronology and its tectonic correlation in the Dabieshan orogen, central China. Sci. China Earth Sci. 48 (4), 506–520.
Xu, C., Zhou, Z., Chang, Y., Guillot, F., 2010. Genesis of Daba arcuate structural belt related to adjacent base-ment upheavals: constraints from Fission-track and (U–Th)/He thermochronology. Sci. China Earth Sci. 53 (11), 1634–1646.
Yang, Z., Courtillot, V., Besse, J., Ma, X., Xing, L., Xu, S., Zhang, J., 1992. Jurassic paleomagnetic constraints on the collision of the north and south China blocks. Geophys. Res. Lett. 19 (6), 577–580.
Yang, K., Liu, S., Li, Q., Wang, Z., Han, Y., Wu, F., Zhang, F., 2009. LA-ICPMS zircon U–Pb geochronology and geological significance of Zhashui granitoids and Dongjiangkou granitoids from Qinling, central China. Acta Sci. Nat. Univ. Pekinesis 45 (5), 841–847 (in Chinese with English abstract).
Yang, Z., Ratschbacher, L., Jonckheere, R., Enkelmann, E., Dong, Y., Shen, C., Wiesinger, M., Zhang, Q., 2013. Late-stage foreland growth of China's largest orogens (Qinling, Tibet): evidence from the Hannan-Micang crystalline massifs and the northern Sichuan Basin, central China. Lithosphere 5 (4), 420–437.
Ye, H., Mao, J., Li, Y., Guo, B., Zhang, C., Liu, W., Yan, Q., Liu, G., 2006. SHRIMP zircon U–Pb and molybdenite Re–Os dating for the superlarge donggou porphyry Mo deposit in East Qinling, China, and its geological implication. Acta Geol. Sin. 80 (7), 1078–1088 (in Chinese with English abstract).
Yin, A., 2010. Cenozoic tectonic evolution of Asia: a preliminary synthesis. Tectonophysics 488 (1–4), 293–325.
Yin, A., Nie, S., 1993. An indentation model for the north and south China collision and the development of the Tan-Lu and Honam fault systems, eastern Asia. Tectonics 12, 801–813.
Yin, A., Nie, S., 1996. A Phanerozoic palinspastic reconstruction of China and its neighboring regions. In: Yin, A., Harrison, T.M. (Eds.), The Tectonic Evolution of Asia. Cambridge University Press, Cambridge, UK, pp. 442–485.
Yin, A., Harrison, T.M., 2000. Geologic evolution of the Himalayan-Tibetan Orogen. Annu. Rev. Earth Pl. Sc. 28, 211–280.
Yin, G., Lu, Y., Zhao, H., Li, W., Li, L., Guo, S., 2001. The tectonic uplift of the Hua Shan in the Cenozoic. Chin. Sci. Bull. 46 (19), 1665–1668.
Yu, X., Liu, J., Zhang, D., Zheng, Y., Li, C., Chen, S., Li, T., 2013. Uprising period and elevation of the Wenyu granitic pluton in the Xiaoqinling district, Central China. Chin. Sci. Bull. 58, 4459–4471.
Yuan, W., Bao, Z., Dong, J., Guo, Z., Deng, J., 2007. Zircon and apatite fission track analyses on mineralization ages and tectonic activities of Tuwu-Yandong porphyry copper deposit in northern Xinjiang, China. Sci. China Earth Sci. 50 (12), 1787–1795.
Zhang, G., Yu, Z., Sun, Y., Cheng, S., Li, T., Xue, F., Zhang, C., 1989. The major suture zone of the Qinling orogenic belt. J. Southeast Asian Earth Sci. 3 (1–4), 63–76.
Zhang, P., Burchfiel, B.C., Molnar, P., Zhang, W., Jiao, D., Deng, Q., Wang, Y., Royden, L., Song, F., 1991. Amount and style of Late Cenozoic deformation in the Liupan Shan area, Ningxia Autonomous Region, China. Tectonics 10 (6), 1111–1129.
Zhang, Y.Q., Vergely, P., Mercier, J., 1995. Active faulting in and along the Qinling Range (China) inferred from spot imagery analysis and extrusion tectonics of south China. Tectonophysics 243 (1–2), 69–95.
Zhang, G., Meng, Q., Yu, Z., Sun, Y., Zhou, D., Guo, A., 1996. Orogenesis and dynamics of the Qinling Orogen. Sci. China Earth Sci. 39 (3), 225–234.
Zhang, Y.Q., Mercier, J.L., Vergély, P., 1998. Extension in the graben systems around the Ordos (China), and its contribution to the extrusion tectonics of south China with respect to Gobi-Mongolia. Tectonophysics 285 (1–2), 41–75.
Zhang, G., Zhang, B., Yuan, X., Xiao, Q., 2001. Qinling Orogenic Belt and continental dynamics. Science Press, Beijing, pp. 1–855 (in Chinese with English abstract).
Zhang, Y., Ma, Y., Yang, N., Shi, W., Dong, S., 2003. Cenozoic extensional stress evolution in North China. J. Geodyn. 36 (5), 591–613.
Zhang, G., Dong, Y., Lai, S., Guo, A., Meng, Q., Liu, S., Cheng, S., Yao, A., Zhang, Z., Pei, X., Li, S., 2004. Mianlue tectonic zone and Mianlue suture zone on southern margin of Qinling-Dabie orogenic belt. Sci. China Earth Sci. 47 (4), 300–316.
Zhang, Z., Zhang, G., Liu, D., Wang, Z., Tang, S., Wang, J., 2006. Isotopic geochronology and geochemistry of ophiolites, granites and clastic sedimentary rocks in the Qinling Orogenic Belt. Geological Publishing House, Beijing, pp. 176–302 (in Chinese).
Zhang, C., Gao, S., Yuan, H., Zhang, G., 2007. Characters of the early Paleozoic mantle in southern Qinling: the Sr–Nd–Pb isotopic evidences of the ultramafic–mafic dykes and volcanic rocks. Sci. China Earth Sci. 37 (7), 857–865.
Zhang, C., Wang, T., Wang, X., 2008. Origin and tectonic setting of the Early Mesozoic granitoids in Qinling Orogenic Belt. Geol. J. China Univ. 14 (3), 304–316 (in Chinese with English abstract).
Zhang, Y., Shi, W., Li, J., Wang, R., Li, H., Dong, S., 2010. Formation mechanism of the Dabashan foreland arc-shaped structural belt. Acta Geol. Sin. 84 (9), 1300–1315 (in Chinese with English abstract).
Zhao, H., Jiang, S., Frimmel, H.E., Dai, B., Ma, L., 2012. Geochemistry, geochronology and Sr–Nd–Hf isotopes of two Mesozoic granitoids in the Xiaoqinling gold district: implication for large-scale lithospheric thinning in the North China Craton. Chem. Geol. 294–295, 173–189.

Please cite this article in press as: Chen, H., et al. Apatite fission-track thermochronological constraints on the pattern of late Mesozoic–Cenozoic uplift and exhumation of the Qinling Orogen, central China. Journal of Asian Earth Sciences (2014), http://dx.doi.org/10.1016/j.jseaes.2014.10.004